

# CHANDRA OBSERVATIONS OF THE GALAXY GROUP AWM 5: COOL CORE RE-HEATING AND THERMAL CONDUCTION SUPPRESSION

A. BALDI, W. FORMAN, C. JONES, P. NULSEN, L. DAVID, R. KRAFT  
Harvard-Smithsonian Center for Astrophysics

AND

A. SIMIONESCU  
Max Planck Institute for Extraterrestrial Physics  
*submitted to ApJ*

## ABSTRACT

We present an analysis of a 40 ksec Chandra observation of the galaxy group AWM 5. It has a small ( $\sim 8$  kpc) dense cool core with a temperature of  $\sim 1.2$  keV and the temperature profile decreases at larger radii, from  $\sim 3.5$  keV just outside the core to  $\sim 2$  keV at  $\sim 300$  kpc from the center. The abundance distribution shows a “hole” in the central  $\sim 10$  kpc, where the temperature declines sharply. An abundance of at least a few times solar is observed  $\sim 15 - 20$  kpc from the center. The deprojected electron density profile shows a break in slope at  $\sim 13$  kpc and can be fit by two  $\beta$ -models, with  $\beta = 0.72^{+0.16}_{-0.11}$  and  $r_c = 5.7^{+1.8}_{-1.5}$  kpc, for the inner part, and  $\beta = 0.34 \pm 0.01$  and  $r_c = 31.3^{+5.8}_{-5.5}$  kpc, for the outer part. The mass fraction of hot gas is fairly flat in the center and increases for  $r > 30$  kpc up to a maximum of  $\sim 6.5\%$  at  $r \sim 380$  kpc. The gas cooling time within the central 30 kpc is smaller than a Hubble time, although the temperature only declines in the central  $\sim 8$  kpc region. This discrepancy suggests that an existing cooling core has been partially re-heated. In particular, thermal conduction could have been a significant source of re-heating. In order for heating due to conduction to balance cooling due to emission of X-rays, the conductivity must be suppressed by a large factor (at least  $\sim 100$ ). Past AGN activity (still visible as a radio source in the center of the group) is however the most likely source that re-heated the central regions of AWM 5. We also studied the properties of the ram pressure stripped tail in the group member NGC 6265. This galaxy is moving at  $M \approx 3.4^{+0.5}_{-0.6}$  ( $v \sim 2300$  km s $^{-1}$ ) through the hot group gas. The physical length of the tail is  $\sim 42$  kpc and its mass is  $2.1 \pm 0.2 \times 10^9 M_\odot$ .

*Subject headings:* conduction – galaxies: clusters: individual (AWM 5) – galaxies: individual (NGC 6269, NGC 6265) – (galaxies:) intergalactic medium – radio continuum: galaxies – X-rays: galaxies: clusters

## 1. INTRODUCTION

The galaxy group AWM 5 (Albert et al. 1977) is an X-ray luminous nearby group ( $z = 0.0348$ ) with  $L_X \sim 6 \times 10^{43}$  erg s $^{-1}$  (Jones & Forman 1999). The cD galaxy NGC 6269 lies at the group center and at the peak of the X-ray surface brightness distribution. NGC 6269 contains a weak central radio source ( $\sim 27$  mJy) with north-south radio lobes ( $\sim 8$  and  $\sim 10$  mJy) extending  $25''$  from the center (Burns et al. 1981, Giacintucci et al. 2007). NGC 6269 dominates the optical light from AWM 5. Since the group member NGC 6265 is only  $\sim 1.3$  mags fainter than NGC 6269 and is located at  $\sim 260$  kpc (in the plane of the sky) from the center, AWM 5 does not strictly follow the criteria of Jones et al. (2003) for the definition of “fossil” groups (e.g. Ponman et al. 1994, Mulchaey & Zabludoff 1999, Jones et al. 2000). However projection effects may increase in principle the distance between the two galaxies pushing it over the half a virial radius limit. Moreover the velocity difference (perpendicularly to the plane of the sky) between NGC 6265 and NGC 6269 is quite high ( $\sim 700$  km s $^{-1}$ ), therefore NGC 6265 is almost certainly not a resident of the group core. In any case NGC 6269 clearly dominates the optical light in AWM 5. Although it does not meet the formal definition of a fossil group given in Jones et al. (2003), AWM 5 is a system with a dominant central

galaxy, making it a group well suitable for a comparison with both “fossil” and normal groups.

In a hierarchical Universe, smaller systems collapse and virialize at an earlier stage than more massive systems. Although smaller density fluctuations also can generate groups of galaxies at later epochs, dense groups should be generally older, more dynamically evolved systems than clusters of galaxies. In galaxy groups, galaxy mergers can occur very efficiently because of their low velocity dispersions, comparable in some cases to the internal velocity dispersion of the individual member galaxies. In an old, relatively isolated group with little subsequent infall, there may be sufficient time for most massive galaxies (but not all the low mass galaxies) to lose energy via dynamical friction and merge, producing a system consisting of a giant central elliptical galaxy, dwarf galaxies and extended X-ray/dark matter halos. This is one of the proposed scenarios for the formation of giant isolated elliptical galaxies and it is based on the galactic cannibalism discussed by Hausman & Ostriker (1978). The observation of “fossil” groups (Ponman et al. 1994) provides clear evidence for the above mechanism. Numerical simulations (Barnes 1989) suggested that a few billion years are required for compact group members to merge and form a single elliptical galaxy.

Presently, about a dozen such systems are identified

(e.g. Ponman et al. 1994, Vikhlinin et al. 1999, Mulchaey & Zabludoff 1999, Jones et al. 2000, Jones et al. 2003) but just a few have been studied in detail (e.g. Khosroshahi et al. 2004, Sun et al. 2004). In a 160 deg<sup>2</sup> ROSAT PSPC survey, Vikhlinin et al. (1999) found four such objects. Computing the volume covered by their survey, they estimated that “fossil” groups represent  $\sim 20\%$  of all clusters and groups with  $L_X > 2 \times 10^{43}$  ergs s<sup>-1</sup>. Consistent results were obtained by Jones et al. (2003) who, using a precise definition of such a system, found that “fossil” groups represent a sizeable percentage (8%-20%) of all systems with comparable X-ray luminosities, and are as numerous as poor and rich clusters combined.

More recently Khosroshahi et al. (2007), using Chandra X-ray observations and optical data of a flux-limited sample of five fossil groups (plus additional systems from the literature), studied in detail the scaling properties of fossils compared to normal groups and clusters. Considering groups having the same optical luminosity, they found that fossils are generally more X-ray luminous than non-fossil groups. In their sample, however, fossil groups follow the conventional  $L_X$ - $T_X$  relation of galaxy groups and clusters, suggesting that the X-ray luminosity and the gas temperature are both increased, as a consequence of their early formation. They also found other signatures of their early epoch of formation such as the higher mass concentration in fossils than in non-fossils, and the  $M_X$ - $T_X$  relation, suggesting that fossils are hotter for a given total gravitational mass. The explanation they give for the difference between fossil and non-fossil properties is that the cuspy potential well in fossils tends to raise the luminosity and temperature of their intergalactic medium (IGM). However, this works together with the lower gas entropy (especially in lower mass systems) compared to normal groups, which could arise from less effective pre-heating of the gas in fossils. Another likely effect of the early shock heating of the IGM is that galaxy formation efficiency is quite low in fossil systems, as suggested by the high mass-to-light ratios observed.

In this paper, we describe the results from a Chandra observation of the galaxy group AWM 5, dominated by the central galaxy NGC 6269. The paper is organized as follows. We first describe the Chandra data preparation and the analysis method in §2. We present the results coming from the X-ray morphology and spectral analysis of the diffuse gas in §3, comparing the optical-IR properties of the galaxies in the group with their X-ray properties in §4. We discuss the results and their implications in §5. The “stripped” galaxy NGC 6265 falling into the group is described in §6, and the conclusions of the paper are drawn in §7.

All the uncertainties are  $1\sigma$  (68%) for one interesting parameter, unless otherwise stated. The abundance estimates are relative to the cosmic values given in Anders & Grevesse (1989). Throughout this paper we assume  $H_0 = 100 h$  km s<sup>-1</sup> Mpc<sup>-1</sup>,  $h = 0.7$ ,  $\Omega_m = 0.3$  and  $\Omega_\Lambda = 0.7$ . For these parameters and a redshift of AWM 5 of  $z = 0.0348$ ,  $1'' \approx 0.67$  kpc.

## 2. CHANDRA DATA PREPARATION AND ANALYSIS

AWM 5 was observed by the ACIS-I detector on-board Chandra on 2003, December 29 for a total of 40 ks (ObsID: 4972). The Chandra data analysis has been per-

formed using CIAO v3.4, which applies the newest ACIS gain maps, the time-dependent ACIS gain correction, and the ACIS charge transfer inefficiency correction. The background light curve during the observation was examined to detect periods of high background following Markevitch et al. (2003a); no significant flaring episodes were detected, giving a total good integration time of  $\sim 39.5$  ks.

### 2.1. Background Subtraction

Since the AWM 5 group fills most of the Chandra field of view, we use the blank-field observations, processed identically to the group observation (i.e. as described above) and reprojected onto the sky using the aspect information from the group pointing. We renormalized the blank-fields to the background of the observation, using the ACIS-S2 chip, in a region of the ACIS field of view practically free from group emission. To perform the normalization, we used the energy band from 9.5 to 12 keV, which is dominated by charged particles.

We followed the procedure of Vikhlinin et al. (2005), to check if the diffuse soft X-ray background could be an important background component in our observation. We extracted a spectrum from the source-free regions of the detector (again the S2 chip), subtracted the renormalized blank-field background and fit the background subtracted spectrum in XSPEC v11.3.2p (in the 0.4-1 keV band) with an unabsorbed *mekal* model, whose normalization was allowed to be negative. The residuals were found to be negligible and consistent with zero, suggesting that an additional soft background correction is not necessary for our dataset.

## 3. RESULTS

### 3.1. X-ray morphology and surface brightness

Figure 1 shows a 0.5-4 keV ACIS-I image of the center of AWM 5. The X-ray peak is coincident with the cD galaxy NGC 6269 (Fig. 2). The group core is clearly visible at the center of the image, and diffuse emission is visible out to several arcminutes from the center. The X-ray tailed galaxy NGC 6265 (a member of the AWM 5 group) is visible on the far west of the image and is the only other group member associated with extended X-ray emission. We performed a radial analysis of the diffuse X-ray emission to determine its properties. We used CIAO *wavedetect* to identify all the  $3\sigma$  point sources and excluded them from the image. To extract a radial profile we used circular annuli of increasing thickness (from 4'' to 20''), out to  $\sim 10'$ . We also computed an exposure map of the observation. The exposure map values were averaged inside each annulus and renormalized to the exposure time in the central annulus.

The background subtracted exposure corrected surface brightness profile of AWM 5 is plotted in Figure 3. A break in the slope of the surface brightness profile is visible in the plot, at  $\sim 10$  kpc from the group center. The surface brightness is well fit at all radii by two  $\beta$  models having core radii of  $r_c = 0.8 \pm 0.1$  kpc and  $r_c = 12.8^{+3.4}_{-0.9}$  kpc in the inner ( $r < 11.4$  kpc) and the outer part ( $r > 11.4$  kpc) respectively ( $\chi^2/dof = 39.8/44$ ). The corresponding best fit values of  $\beta$  are  $0.458^{+0.014}_{-0.013}$  and  $0.357 \pm 0.002$ , respectively.

To check for anisotropies in the X-ray emission we

extracted radial profiles in four azimuthal sectors (see Fig. 4). The procedure adopted to compute the surface brightness was the same described above for the overall radial profile. We fit a  $\beta$  model to each sector at  $r > 10$  kpc (see Table 1). While the northern and the western sectors are clearly well described by single  $\beta$  models, the southern and the eastern surface brightness profiles are slightly more deviant. However the deviations are statistically insignificant ( $\chi^2/\nu = 34.2/26$  and  $\chi^2/\nu = 37.7/26$ , respectively).

### 3.2. Mean Temperature and Virial Radius

The virial radius  $r_{180}$  of AWM 5 can be estimated from:

$$r_{180} = 1.95h^{-1} (\langle kT \rangle / 10 \text{ keV})^{1/2} (1+z)^{-3/2} \text{ Mpc} \quad (1)$$

(Evrard et al. 1996) This scaling relation may not be valid for cool groups (see e.g. Sanderson et al. 2003) but can still be used for comparison with other work (see § 3.7 below). To compute the global temperature  $\langle kT \rangle$  necessary to estimate  $r_{180}$ , we extracted a spectrum from  $0.05r_{180}$  to  $0.3r_{180}$ . The central region is excluded to avoid contamination from the group cooling core (CC). The spectra were fitted in XSPEC v11.3.2p with a single temperature *mekal* model, with Galactic absorption ( $4.8 \times 10^{20} \text{ cm}^{-2}$ ; Stark et al. 1992) leaving the metal abundance free to vary. The values of  $\langle kT \rangle$  and  $r_{180}$  are evaluated iteratively until convergence to a stable value of the temperature is obtained ( $\Delta kT \leq 0.01$  keV between two different iterations). The best fit temperature was  $kT = 2.33^{+0.39}_{-0.19}$  keV, while the best fit metallicity was  $Z = 0.40^{+0.22}_{-0.13} Z_{\odot}$ . The virial radius estimated from eq. 1 for AWM 5 is  $r_{180} = 1.28$  Mpc. The total X-ray luminosity observed within the emission region ( $r < 400$  kpc) is  $\sim 1.3 \times 10^{43} \text{ erg s}^{-1}$ . At  $r_{500}$  (1.03 Mpc) and at  $r_{180}$  the total luminosities, extrapolated from the surface brightness  $\beta$  model fit (§ 3.1), are  $\sim 1.6 \times 10^{43} \text{ erg s}^{-1}$  and  $\sim 1.7 \times 10^{43} \text{ erg s}^{-1}$ , respectively.

### 3.3. Temperature and Abundance profiles

To study the physical properties of the group emission, we subdivided the emission from the group into annuli centered on the X-ray peak. We required  $\sim 1,000$  net counts in each of the central annuli ( $r < 40$  kpc), and  $\sim 2,000$  net counts in each of the outer annuli ( $r > 40$  kpc), where the surface brightness is lower and the contribution from the background is higher. We extracted a spectrum from each annulus (excluding point sources) using *specextract*, which generates source and background spectra and builds appropriate RMFs and ARFs. The background is taken from the re-normalized blank field observations using the same region as the source.

The spectra were analyzed with XSPEC v11.3.2p (Arnaud et al. 1996) and fitted with a single-temperature *mekal* model (Kaastra 1992; Liedahl et al. 1995). The free parameters in the model are the gas temperature  $kT$ , the gas metallicity  $Z$  and the normalization. The spectral band considered is 0.5–4 keV. All the spectra were rebinned to have at least 20 counts per bin. We have measured  $N_H$  from the X-ray data, finding it consistent (within  $1\sigma$ ) with the Galactic value along the line of sight, as derived from radio data ( $4.8 \times 10^{20} \text{ cm}^{-2}$ ; Stark et al. 1992). Since the presence of AGN activity in the center of AWM 5 is very likely, we have tried to add an

additional power-law component to the thermal model in the central annulus. The fit is not improved significantly by the presence of the additional spectral component ( $\Delta\chi^2_{\nu} < 0.05$ ) and the contribution of a power-law is  $< 10\%$  of the thermal component. We also considered an image in the 3–8 keV band, finding that no hard point-like emission is present both in the Chandra 40ks observation and in an off-axis XMM archival observation (centered on NGC 6264, PI: Greenhill).

The projected temperature and abundance profiles of AWM 5 are shown in Figure 5.

The temperature profile shows the presence of an  $\sim 8$  kpc-sized CC (projected  $kT \sim 1.3$  keV; de-projected  $kT \sim 1.2$ ) with the profile having a peak just outside the core and then declining from  $\sim 3$  keV to  $\sim 2$  keV at larger radii. The abundance profile is suggestive of a “hole” in the center coincident with the CC. The abundance value rises just outside the core reaching a maximum of a few times solar at a radius of  $\sim 15 - 20$  kpc and then declines to subsolar values. The probability that the value of the abundance is the same in the inner two bins and that the “hole” is produced by statistical fluctuations is  $\sim 1\%$  and  $\sim 0.3\%$  in the projected and deprojected case, respectively. Similar behaviour is observed in other groups and clusters of galaxies (e.g. Perseus cluster; Schmidt et al. 2002; Churazov et al. 2001; 2002) and was observed in “fossil” groups (e.g. ESO 3060170; Sun et al. 2004).

We also examined the radial variation of Si, S and Mg fitting a *vmekal* single temperature model to the radial annuli. The Fe and Mg abundance show a trend very similar to what was observed in the metal abundance profile in the *mekal* fit. On the other hand S and Si abundances are constant within the errors, although the large statistical errors cannot exclude that these abundances could follow the same radial trend as the other metals. The data quality does not allow a direct comparison of the SNIa and SNII product yields with the results coming from the study of Rasmussen & Ponman (2007) on a large sample of galaxy groups.

### 3.4. Physical Parameters

The electron density profile can be obtained by deprojecting the surface brightness profile (see e.g. David et al. 2001; Sun et al. 2003). Based on the ROSAT All-Sky Survey, we determined that the flux contribution from regions beyond the outermost bin ( $\sim 10'$ ) is not significant. Thus the “onion-peeling” technique adopted starts in the outer annulus, converting the observed background-subtracted and exposure-corrected 0.5–4 keV surface brightness profile (derived in 22 radial bins) to electron density. In each bin, an emissivity for the gas at a fixed temperature  $kT$  and  $Z$  is computed for a standard *mekal* model to perform the conversion. The procedure determines the density at progressively smaller radii, subtracting the projected emission from larger radii. In the temperature range observed in the projected profile of AWM 5 ( $1.3 \leq kT \leq 3.2$  keV), the X-ray emissivity is sensitive to both abundance and temperature. Therefore, with the assumption of spherical symmetry, we first performed a spectral deprojection to obtain the 3D temperature and abundance profiles (Fig. 5). Only six radial bins were considered for the spectral deprojection. Because of the steep temperature gradient observed in the core of AWM 5 we chose a broken power-law model to fit

$kT$ . A second order polynomial was chosen to model the radial dependence of the abundance. We varied the values of  $kT$  and  $Z$  within their  $1\sigma$  uncertainties, through 1000 Monte Carlo simulations to obtain the  $1\sigma$  errors on the best-fit parameters of the fits to the  $kT$  and  $Z$  profiles. The statistical errors in the electron density were determined by combining the uncertainties in the X-ray emissivity and in the surface brightness profiles. The missing emission volume in each annulus because of the chip edges, gaps and point sources was derived by Monte Carlo simulations and included in the computation of the errors as well.

The derived electron density profile is shown in Fig. 6. It can be fit by a double  $\beta$ -model although the best-fit  $\chi^2$  is not good ( $\chi^2/dof = 47.0/16$ ), mostly because of the three points at  $25 \text{ kpc} < r < 60 \text{ kpc}$ . The inner  $\beta$ -model (at  $r < 13.4 \text{ kpc}$ ) has best fit values of:  $\beta = 0.72^{+0.16}_{-0.11}$ ;  $r_c = 5.7^{+1.8}_{-1.5} \text{ kpc}$ . A core radius of  $r_c = 31.3^{+5.8}_{-5.5} \text{ kpc}$  and a  $\beta = 0.34 \pm 0.01$  were derived for the outer  $\beta$ -model (at  $r > 13.4 \text{ kpc}$ ). At  $r > 30 \text{ kpc}$  a power-law can also be fit to the data ( $\chi^2/dof = 33.3/15$ ). We found that  $n_e \propto r^{-0.91 \pm 0.02}$  between 30 kpc and 300 kpc. The slope measured for the density profile is very similar to that observed in cool groups (e.g. NGC1550, Sun et al. 2003) but much flatter than those measured in “fossil” groups (e.g. NGC6482, Khosroshahi et al. 2004; ESO3060170, Sun et al. 2004) and in clusters, where generally  $n_e \propto r^{-2}$  beyond several core radii. With the deprojected electron density profile, we were also able to derive the cooling time and entropy profiles (defined as  $S = kT/n_e^{2/3}$ ; Fig. 7). The cooling time is less than  $10^9 \text{ yr}$  in the very center and less than a Hubble time ( $\sim 10^{10} \text{ yr}$ ) within the central 30 kpc.

### 3.5. Energetics of the radio lobes

As described in § 1, AWM 5 hosts a weak central radio source (Fig. 8). The two lobes seem to be coincident with a depression in the X-ray emission, observed especially in the southern lobe. However the Chandra data are not sufficiently deep to perform any detailed analysis on such cavities.

From the geometrical properties of the radio lobes and the density and temperature (and hence pressure) profiles derived above we can determine some of their physical parameters. The calculations derived in this section refer to the northern radio lobe, however the two lobes are quite symmetric and we can consider these numbers valid also for the southern lobe. The northern lobe shape can be approximated with a sphere with a  $\sim 8''$  radius ( $\sim 5.4 \text{ kpc}$ ). We assume that the lobe rose buoyantly at half the speed of sound (e.g. as in M 87, Churazov et al. 2001). At the temperature of the CC of AWM 5,  $kT = 1.2 \text{ keV}$ , the speed of sound is  $c_s \sim 600 \text{ km s}^{-1}$ , the rise time of the lobe and hence the age is therefore  $3.5 \times 10^7 \text{ yr}$ , consistent with the radiative age  $t_{rad} = 6.5 \times 10^7$  derived by Giacintucci et al. (2007). The energy necessary to inflate the lobe can be calculated as  $4pV$  ( $p$  is the local hot gas pressure since the lobe is supposed to be in pressure equilibrium, and  $V$  is the volume of the lobe itself) and is  $6.4 \times 10^{57} \text{ erg}$ . Therefore the power necessary to inflate the lobe in  $3.5 \times 10^7 \text{ yr}$  is  $\sim 5.8 \times 10^{42} \text{ erg s}^{-1}$ . This number is two orders of magnitude higher than the X-ray upper limit we obtain

for the AGN at the center of NGC 6269. If we estimate the mechanical luminosity of the rising bubble as  $L_{mech} = pV/t$  (Bîrzan et al. 2004), where  $t$  is the age of the bubble, we obtain  $L_{mech} \sim 1.4 \times 10^{42} \text{ erg s}^{-1}$ . This can also be compared with a total radio luminosity of  $\sim 10^{40} \text{ erg s}^{-1}$  (see § 5), in agreement with the  $L_{radio} - L_{mech}$  relation derived by Bîrzan et al. (2004), who find that  $L_{mech} \gg L_{radio}$ .

Marconi & Hunt (2003) derived a correlation between the bulge infrared luminosity ( $L_{K_s, bulge}$ ) and the mass of the central black hole ( $M_{BH}$ ). For NGC 6269 we estimate  $M_{BH} \sim 10^9 M_\odot$ . The luminosity expected for steady Bondi accretion (Bondi 1952; see § 4.1) of a  $10^9$  solar masses black hole (deriving the density at  $r = 0$  from the inner  $\beta$ -model obtained in § 3.4) is at least one order of magnitude larger than the energy necessary to inflate the radio bubbles.

If the radio-lobes are not parallel to the plane of the sky the estimates performed above will be different. In particular, if we name  $\theta$  the inclination angle of the lobe axis with respect to the plane of the sky, the volume of the bubble will be increased by a factor  $(\cos \theta)^{-1}$  and so the energy necessary to inflate the bubble. However, unless we are dealing with a very extreme inclination angle, the estimates computed in this Section can be considered reliable within a factor of a few.

### 3.6. X-ray Gas Mass and Total Gravitating Mass

The gas density and temperature profiles derived in § 3.4 can be used to estimate the total gravitational mass profile under the assumption of hydrostatic equilibrium:

$$M(< r) = -\frac{kT(r)r}{\mu m_p G} \left( \frac{d \log n_e(r)}{d \log r} + \frac{d \log T(r)}{d \log r} \right) \quad (2)$$

where  $G$  and  $m_p$  are the gravitational constant and proton mass, and the mean particle mass is  $\mu = 0.6$ . Following a procedure similar to that applied in § 3.4 in the deprojection of the surface brightness profile, we considered the broken power-law functional  $kT(r)$  as derived in § 3.4. We perturbed the value of  $kT(r)$  within its  $1\sigma$  uncertainties, through 1000 Monte Carlo simulations. For the electron density profile we assumed the double  $\beta$ -model described above in § 3.4 and a similar method was applied to derive the density gradient and its uncertainties. The derived uncertainties were combined to compute the errors for the total gravitating mass profile. Both the total mass and gas mass profiles are shown in Fig. 9, along with the gas mass fraction. In these plots, we did not show the CC region ( $r < 10 \text{ kpc}$ ) in which the determination of the mass is obviously more difficult because of the strong temperature gradient.

The total mass within the central 15 kpc is quite high ( $\sim 10^{12} M_\odot$ ), a value higher than those usually observed in groups (see e.g. Gastaldello et al. 2007). However AWM5 is a hot group and the high mass concentration in the center is most likely due to the presence of the central massive galaxy NGC6269, whose hot gas halo is superimposed over the group halo. We fitted a Navarro, Frenk & White (1996; NFW) profile to measure the concentration parameter  $c_{200}$  as in Khosroshahi et al. (2007). A single NFW fit cannot account for the shape of the mass profile at all radii. This can be explained by superposition of two halos of dark matter from the group and from the central galaxy NGC 6269. Moreover complications could

be introduced by the radio source (which could be more extended than visible in the FIRST) and by the presence of a steep gradient in temperature. Fitting the inner part ( $r < 80$  kpc) we obtain an unusual concentration parameter  $c_{200} \sim 100$ . On the other hand, if we fit the outer part ( $r > 80$  kpc) we obtain a more reasonable  $c_{200} \sim 20$  which in a  $M$  vs.  $c_{200}$  diagram falls in the region occupied by other groups (e.g. the RXJ0454.8-1806 group; Khosroshahi et al. 2007).

The gas mass fraction has a constant value ( $\sim 0.05\%$ ) at  $10 \text{ kpc} < r < 30 \text{ kpc}$ , starting to increase rapidly at  $r > 30 \text{ kpc}$ . The gas fraction reaches a maximum value of  $\sim 6.5\%$  at  $\sim 380 \text{ kpc}$ , with no obvious signs of flattening at large radii. For comparison, typical gas fractions at large radii are  $\sim 15\%$  in clusters (e.g. David et al. 1995) and  $\sim 5\%$  in groups (Gastaldello et al. 2007). In the “fossil” group ESO3060170 (Sun et al. 2004) the gas fraction is  $\sim 5\%$  at  $r = 200 \text{ kpc}$  and stops growing after that radius. In AWM5,  $f_{gas}$  is  $\sim 2.5\%$  at  $r = 200 \text{ kpc}$ , however it shows a trend to increase even at  $r > 380 \text{ kpc}$  and it might converge to a larger value than observed with the Chandra data.

### 3.7. Entropy profile

The entropy profile of AWM 5 can be compared with those of other groups. We plot the scaled entropy profiles ( $(1+z)^2 T^{-0.65} S$ ) of AWM 5 and three other groups in Fig. 10: ESO 3060170 (Sun et al. 2004) NGC 5419 and NGC 6482 (Khosroshahi et al. 2004). The scaled profile of AWM 5 is clearly flatter than all but NGC 5419. Simulations and analytical models of spherical accretion onto clusters predict entropy profiles with a  $S \propto r^{1.1}$  (Tozzi & Norman 2001), at least outside the central region (where heating and cooling are important). However, in the case of AWM 5, the entropy profile is never consistent with such a slope. The entropy is better described by a slope  $S \propto r^{0.7}$ .

At  $0.01 r_{180} < r < 0.04 r_{180}$  a further flattening of the profile is observed, similar to what is observed in ESO 3060170 and NGC 5419. This variety of inner entropy profiles is generally related to the evolutionary stages of group CCs. Groups with heated gas cores can have flat inner entropy profiles (see e.g. AWM 4, O’Sullivan et al. 2005), while those with large CCs do not have flat entropy cores. In the case of AWM 5 the flattening of the entropy, at least in the inner part, is coincident with the position of the X-ray cavities generated by the two radio-lobes. However the flattening extends far beyond those cavities and most likely is directly related to the re-heating of the CC (see § 5).

## 4. OPTICAL-IR PROPERTIES VS. X-RAY PROPERTIES

Figure 11 shows the ESO Digitized Sky Survey image (R band) of the central regions of AWM 5. Galaxies with measured radial velocities (from Koranyi & Geller 2002) consistent with that of the group are labelled. Apart from NGC 6269 (the dominant galaxy in AWM 5) and NGC 6265 (see § 6), only three of the 12 group galaxies in the Chandra field of view are detected in the X-rays. Two other X-ray sources within  $1'$  ( $\sim 40 \text{ kpc}$ ) of NGC 6269 have red, galaxy-like optical counterparts and are likely group members. These two objects together with the galaxy D4 are listed in Table 2. Their optical colors ( $u - g = 2.5$ ;  $g - r = 1.4$ ,  $r - i = 1.1$ ) rule out the possibility

that they could be background AGN (see e.g. Richards et al. 2001). These values put them in the region of the color-color diagrams of late M-type stars (Finlator et al. 2000), and are very different from the colors observed in all the other galaxies of the group ( $1.7 < u - g < 2.0$ ;  $0.8 < g - r < 0.9$ ,  $0.4 < r - i < 0.5$ ). The presence of a Chandra counterpart excludes the possibility that we are observing two red giants and suggests that we are dealing with very old stellar systems.

We compared the X-ray and infrared luminosities of the galaxies in AWM 5 with a bright nearby sample of early-type galaxies (Ellis & O’Sullivan 2006). The X-ray luminosity (where there is no detection) was computed from the background level detected in a  $3''$  circle centered on the optical position of each galaxy, after modeling out the general group emission at that radius (from the  $\beta$  model derived in § 3.1). Following Poisson’s formula we estimated the number of counts that would be necessary to get a  $3\text{-}\sigma$  detection to obtain a flux and therefore a luminosity. Following a procedure similar to that adopted by Revnivtsev et al. (2008) in the case of the unresolved X-ray emission in NGC 3379, in Figure 12 we plotted the  $K_s$ -band luminosities (expressed in solar units) together with the ratio of the x-ray luminosity over the  $K_s$ -band luminosity, for both the galaxies in AWM 5 and the sample of Ellis & O’Sullivan (2006). A reference value for the maximum expected contribution to the X-ray emission coming from CVs and normal stars (solid line) and from low mass X-ray binaries (LMXBs, dotted line) is shown in the plot as well. The AWM 5 members follow the distribution of early-type galaxies from the bright sample. This is true also for the two galaxies D2 and D3, assuming they are group members. It is clear from this plot that CVs and stars cannot account for the X-ray emission in any of the AWM 5 members. While the X-ray emission from D1 could be due entirely to unresolved LMXBs, the X-ray emission from D2, D3, D4 and D5 is clearly of nuclear origin. Based on their upper limits we cannot exclude that also the other group members with undetected X-ray emission could harbor a nuclear source.

### 4.1. Black hole masses and Bondi accretion rates

In the cores of early-type galaxies, stellar mass loss is of the order of a few  $10^{-5}$  up to a few  $10^{-4} M_{\odot} \text{ yr}^{-1}$  (e.g. Soria et al. 2006) and in most cases represents the most important fueling source for their central black holes (usually larger than the fuel available from the hot gas). For the AWM 5 group members, we estimated the size of the black hole and the amount of fuel available from the X-ray emitting gas following the  $L_{K_s, \text{bulge}} - M_{BH}$  relation of Marconi & Hunt (2003; as done in § 3.5 for NGC 6269). Assuming that all the  $K_s$  luminosity in our galaxies comes from a bulge, we estimated  $M_{BH}$  for all the AWM 5 members. The values of  $M_{BH}$  are presented in Table 3, together with the corresponding ratio between the observed X-ray luminosity  $L_X$  (which can be considered of nuclear origin in all galaxies except for D1) and the expected Eddington luminosity  $L_{Edd}$  for a black hole of mass  $M_{BH}$ . For our sample of AWM 5 group members,  $L_X/L_{Edd} < 5 \times 10^{-6}$  showing that all the black holes are accreting at a highly sub-Eddington rate. Considering the electron density profile of the X-ray emitting gas (as determined in § 3.4) and the temperature profile

of the gas, we estimated the accretion rate on the SMBH, from the Bondi (1952) formula:

$$\dot{M}_{Bondi} = 1.66 \times 10^{-7} M_7^2 T_2^{-3/2} n_{0.1} M_\odot \text{ yr}^{-1} \quad (3)$$

where  $M_7$  is the  $M_{BH}$  in units of  $10^7 M_\odot$ ,  $T_2$  is the temperature in units of 2 keV and  $n_{0.1}$  is the density in units of  $0.1 \text{ cm}^{-3}$ . Assuming an accretion efficiency of  $\eta = 0.1$  we derived the corresponding Bondi luminosity. However, it is worth noting that we do not have any information on the line of sight position of the galaxies, therefore both the Bondi accretion rate and its associated luminosity can only be estimated as upper limits, apart from the case of NGC 6269. Another caveat to take into consideration is that motion of the galaxies through the group gas reduces the accretion rate. Allowing for uncertainties in the accretion rate, it is quite clear that accretion from group hot gas is not important compared to stellar mass loss ( $> \text{a few } 10^{-5} M_\odot \text{ yr}^{-1}$ ; e.g. Soria et al. 2006) in the AWM 5 group members.

#### 5. RE-HEATING MECHANISMS AND THERMAL CONDUCTION SUPPRESSION IN THE COOLING-CORE OF AWM 5

As shown in Fig. 7, the gas cooling time within the central 30 kpc of AWM 5 is less than the Hubble time. However, this group harbors a small dense  $\sim 8$  kpc CC but lacks a group-sized CC which is found in other relaxed groups (e.g., NGC 1550, Sun et al. 2003; MKW 4, O’Sullivan et al. 2003). Also “fossil” groups, which are believed to be old and relaxed systems, are expected that a group-sized CC should develop in the center in a relatively short time (i.e. a few Gyr). Examples of “fossil” groups presenting a smaller CC than expected from the cooling time derived in their central regions are indeed ESO306170 (Sun et al. 2004) and NGC 6482 (Khosroshahi et al. 2004).

The lack of a group-sized CC in AWM 5 can be reconciled with the current age of the system, if an existing CC has been re-heated. Three viable sources for reheating CCs in groups and clusters are energy from mergers (which drive gas motions in the core), energy input from SMBH outbursts in the central galaxy and thermal conduction.

##### 5.1. Thermal conduction

While conduction may be effective at larger radii (e.g., Narayan & Medvedev 2001; Zakamska & Narayan 2003), it is not effective within all cluster (and group) cores. Since CC clusters have a positive temperature gradient, heat can be conducted inward toward the center, balancing the radiative cooling and arresting or retarding the formation of the CC (e.g. Stewart et al. 1984; Bregman & David 1988; Brighenti & Mathews 2002), although this is usually an unstable process.

Gas with temperature  $T$ , density  $n$ , and a volume  $V$  put in thermal contact with an ambient gas having temperature  $T + \Delta T$ , over a contact surface having an area  $A$  will eventually reach thermal equilibrium with the surrounding gas in a time  $\tau$  which can be estimated as (from Böhringer & Fabian 1989, adapted to the 3-D case by e.g. Simionescu et al. 2008):

$$\tau \approx \frac{\Delta H}{qA} \approx \frac{\frac{5}{2}nk\Delta T}{fk_0T^{5/2}\nabla T} \frac{V}{A} \quad (4)$$

where  $\Delta H$  is the enthalpy that needs to be transferred to the lower temperature gas to reach thermal equilibrium,  $q$  is the conductive heat flux,  $f$  is a reduction coefficient that takes into account suppression of heat conduction by magnetic fields, and  $k_0 \sim 6 \times 10^{-7} \text{ erg cm}^{-1} \text{ s}^{-1} \text{ K}^{-7/2}$  is the Spitzer conduction coefficient (Spitzer 1962). For AWM 5, we have a gas temperature  $kT = 1.2$  keV in a sphere with an  $\sim 8$  kpc radius, in contact with ambient gas with a temperature of 3.7 keV. For  $f = 1$ , a density  $n = 0.05 \text{ cm}^{-3}$  and a temperature gradient which is the difference in temperature between the core and the bin right outside the core divided by the distance between the center of the two bins, we obtain a very short timescale of  $\sim 17 \pm 3$  Myr to reach thermal equilibrium between the two gases. Moreover, the conductive heat flux is  $\sim 7 \times 10^{43} \text{ erg s}^{-1}$ , about  $\sim 100$  times larger than the luminosity emitted in X-rays from the core. Both of these facts require a large suppression of the thermal conductivity in the core of AWM 5, by a factor of at least  $\sim 100$ . Such a large suppression factor is predicted by some theoretical calculations (e.g. Rechester & Rosenbluth 1978; Chandran & Cowley 1998) and supported by observations in other clusters and groups of galaxies (e.g. Coma; Vikhlinin et al. 2001b). This is also consistent with the results of Simionescu et al. (2008) for M87.

##### 5.2. Gas sloshing

“Sloshing” of the gas in the group core, generated by past merger activity, could provide enough energy to heat the gas in this region (see e.g., Churazov et al. 2003 for the case of Perseus). Markevitch et al. (2003b) found that approximately 2/3 of relaxed, centrally peaked clusters with CC showed sharp surface brightness discontinuities or “edges”, characteristic of gas motions. After accounting for clusters with “edges” not favorably oriented for detection, all CC clusters likely harbor such features. Ascasibar & Markevitch (2006) argue that in centrally peaked systems, “edges” (or cold fronts) are driven by mergers and that merger driven “sloshing” is long lived since the dark matter does not relax quickly. However, signatures of such merger activity (e.g. surface brightness “edges”) are not clearly visible in the X-ray morphology of AWM 5. The only discontinuities visible in the surface brightness profile are of very low statistical significance and even in the azimuthal profiles the discrepancies from a  $\beta$  model are within the errors. This explanation cannot be accurately tested with the present data and would need a deeper observation to confirm or rule out the “sloshing” as a possible re-heating source of the CC of AWM 5.

##### 5.3. Central SMBH outbursts

Chandra observations have shown buoyant bubbles and weak shocks around central cluster galaxies powered by AGN outbursts (e.g. Perseus, Fabian et al. 2003; M87, Forman et al. 2005). Churazov et al. (2001, 2002) argued that cyclical outbursts from self-regulated accretion onto the central black hole could be the source of energy to (re)heat the CCs. Thus, a central AGN outburst might provide the required energy to heat the outer regions between 8 kpc and 30 kpc. Although the presence of a central AGN is not directly observed in the X-ray data ( $L_X < 5.4 \times 10^{40} \text{ erg s}^{-1}$ ), it is very likely that NGC 6269

harbors a now dormant  $10^9$  solar mass black hole (from its large  $K_s$  band luminosity). As described in § 3.5 a weak radio source is present at the center of NGC 6269 with a total flux (core plus lobes) of  $\sim 45$  mJy at 1400 MHz. Assuming the spectral shape in the radio derived by Giacintucci et al. (2007), we can compute a total radio luminosity (10 MHz - 10 GHz) of  $\sim 9 \times 10^{39}$  ergs  $s^{-1}$ . Taking the relation of Birzan et al. (2004), radio sources with this total luminosity can have mechanical luminosities up to  $2 \times 10^{43}$  ergs  $s^{-1}$ . If the central AGN has been active for the past  $10^8$  yr (consistent with the age of the radio source derived in § 3.5 from the extension of the lobes and with the radiative age determined by Giacintucci et al. 2007), we need a heating rate of  $\sim 3 \times 10^{43}$  ergs  $s^{-1}$ , consistent with the  $2 \times 10^{43}$  ergs  $s^{-1}$  obtained from the radio properties of the group. Therefore, it is possible that a central AGN outburst could be partly responsible for re-heating the gas between 8 and 30 kpc. A signature of this process may also be seen in the entropy profile (Fig. 10). The lower entropy gas between 8 and 30 kpc could have been removed by the AGN outburst (e.g. Brüggen & Kaiser 2002). Moreover, the lifetime of the radio synchrotron emission is only  $24 (B/10 \mu G)^{-3/2} (\nu/1.4 \text{ GHz})^{-1/2}$  Myr after the last injection of relativistic electrons from the nucleus. In this scenario the energy transported by the radio jets was deposited beyond 8 kpc (consistent with the observed extension of the radio lobes) and heated the CC only beyond that radius. Weak shocks could maintain the temperature of the gas at smaller radii (see e.g. Forman et al. 2007, McNamara & Nulsen 2007, for recent examples).

## 6. THE RAM-PRESSURE STRIPPED TAIL IN NGC 6265

Fig. 13 shows signs of possible ram pressure stripping of the atmosphere from the group member NGC 6265, an S0 galaxy. The trailing stream of hot gas is at least 40 kpc long (in the plane of the sky).

The surface brightness profile (Fig. 14) shows a sudden drop (of a factor of 3 – 4 at least) in coincidence with the leading edge of the x-ray emission, while going toward the tail the decrease in surface brightness is definitely more gradual. We extracted spectra in two different regions in the galaxy, one coincident with the core and a rectangular region coincident with the tail. We fit a thermal *mekal* model to the core of the galaxy, obtaining a temperature  $kT = 0.78^{+0.12}_{-0.08}$  keV (with  $Z$  fixed at 0.3 solar). For the tail, we measure  $kT = 0.63^{+0.09}_{-0.07}$  keV ( $Z \equiv 0.3Z_\odot$ ). A second thermal component (with  $kT \equiv 1.8$  keV, as measured from the temperature profile at the radial distance of NGC 6265) was necessary to take into account the contribution from the ICM of AWM 5. The gas temperature observed in the tail is consistent with the temperature present in the core, and more than  $\sim 2$  times lower than the AWM 5 gas at the radial distance of the galaxy, supporting a scenario where this is predominantly ram pressure stripped gas coming from NGC 6265 instead of ICM gas concentrated in the wake. We followed Vikhlinin et al. (2001a) to determine the speed of NGC 6265 with respect to the ambient ICM. The ratio of the pressure  $p_0$  measured at the stagnation point (at the edge of the discontinuity) to the pressure  $p_1$  measured in the free-stream, i.e. in the undisturbed AWM 5 ICM, is directly related to the Mach number  $M$

of the NGC 6265 motion relative to the ICM (Landau & Lifschitz 1959; Vikhlinin et al. 2001a). Although the gas pressure at the stagnation point cannot be measured directly, it must equal the pressure within the leading edge. We assume indeed that the pressure at the stagnation point is equal to the pressure measured in a region including the core of the galaxy, i.e.  $p = 5.2 \pm 1.0 \times 10^{-11}$  dyn  $cm^{-2}$ . A more precise estimate would be to measure the pressure in a thin arc located along the leading edge. However, the counts are too few to perform such a measure. The ratio to the pressure measured in the ICM is  $p_0/p_1 = 17.3^{+5.6}_{-5.3}$ , which corresponds to a Mach number  $M = 3.4^{+0.5}_{-0.6}$ .  $M \gtrsim 3$  requires the presence of a shock front with a density jump of a factor of 3. The surface brightness profile observed in NGC 6265 shows a drop corresponding to the leading edge, consistent with such a scenario (Fig. 14). We derive that the total velocity at which NGC 6265 is moving relatively to the ICM is  $v \sim 2300$  km  $s^{-1}$ . This very high 3D velocity is a further confirmation that NGC 6265 is not a resident of the AWM 5 core (§ 1) Based on the redshift of AWM 5 and NGC 6265 the velocity along the line of sight is  $\sim 700$  km  $s^{-1}$ , therefore the component of the velocity parallel to the plane of the sky is  $\sim 2200$  km  $s^{-1}$  and the inclination angle of the motion of the galaxy with respect to the plane of the sky is  $\xi \sim 18^\circ$ . The physical length of the tail should be then  $\sim 42$  kpc and the ram pressure exerted by the ICM on the NGC 6265 gas because of the supersonic motion through it is  $p_{ram} \sim 4 \times 10^{-11}$  dyn  $cm^{-2}$ . Unfortunately the number of photons detected in this observation (about 300 in the core and in the tail combined) is not sufficient for a detailed analysis. However, we derive the mean gas density, assuming that the tail is a cylinder with an  $18^\circ$  inclination to the plane of the sky. The gas density derived from the spectral analysis is  $n_e = 4.1 \pm 0.3 \times 10^{-3}$   $cm^{-3}$ , at least one order of magnitude denser than the ICM gas ( $n_{e,ICM} < 3 \times 10^{-4}$   $cm^{-3}$ ). The mass of the tail, derived assuming cylindrical geometry, is  $2.1 \pm 0.2 \times 10^9 M_\odot$ .

## 7. DISCUSSION

As discussed in § 5, AWM 5 is harboring a dense  $\sim 8$  kpc sized CC, smaller than expected from the cooling time derived in its central regions. The required energy to heat the 1.2 keV gas (observed in the core at  $r < 8$  kpc) between 8 and 30 kpc to the observed value ( $kT \sim 3.7$  keV) is estimated to be  $\sim 10^{59}$  ergs.

Such a large amount of energy cannot be clearly produced by star formation activity in the central galaxy NGC 6269 which is a cD with practically no ISM detected (e.g. Bettoni et al. 2003). SNIa explosions could be in principle another heating source. If we consider the average supernova rate observed in elliptical galaxies (Turatto et al. 1994) rescaled to the B-band luminosity of NGC 6269 we obtain a rate of 0.89 SN every 100 yr. Considering that each supernova could produce an energy up to  $10^{51}$  ergs we obtain a corresponding heating rate of  $\lesssim 2.8 \times 10^{41}$  erg  $s^{-1}$ . To obtain a total energy of  $\sim 10^{59}$  ergs we would have need a constant supernova rate for more than 10 Gyr. Therefore we can affirm that the contribution of SN to the heating of the gas around the AWM 5 core is negligible. As explained in § 5.2, signatures of “sloshing” of the gas in the group core, generated by past merger activity (e.g. surface brightness

“edges”) could not be found in the X-ray observations of AWM 5. Only deeper data could provide a meaningful test of the importance of sloshing as a re-heating source for the CC of AWM 5.

The only two sources which could have played an important role in the CC re-heating are the thermal conduction and the central SMBH outburst. The observed temperatures in the center of AWM 5 yields a short timescale of  $\sim 17$  Myr to reach thermal equilibrium between the lower temperature gas in the core and the higher temperature gas between 8 and 30 kpc. Moreover, the heat flux expected corresponds to  $L \sim 7 \times 10^{43}$  erg s $^{-1}$ , about  $\sim 100$  times larger than the luminosity emitted in X-rays from the core ( $\sim 5 \times 10^{41}$  erg s $^{-1}$ ). It is clear that these two gases cannot stay in the current equilibrium situation if a large suppression of the thermal conductivity in the core of AWM 5 (by a factor of at least  $\sim 100$ ) is not present. Large suppression factor are indeed predicted by theory (e.g. Chandran & Cowley 1998) and observed in galaxy clusters and groups (e.g. Coma; Vikhlinin et al. 2001b). The most likely scenario is that thermal conduction has been suppressed by a large factor (most likely because of the presence of magnetic fields) and did not contribute significantly to CC re-heating. A central AGN is not directly observed in the AWM 5 X-ray data ( $L_X < 5.4 \times 10^{40}$  erg s $^{-1}$ ). However the  $K_s$  band luminosity suggests that NGC 6269 is harboring a now dormant  $10^9$  solar mass black hole. As a further confirmation to this scenario, a weak radio source is detected in the center of NGC 6269 (see § 3.5). As estimated in § 5.3 a radio source with a total radio luminosity (10 MHz - 10 GHz) of  $\sim 9 \times 10^{39}$  ergs s $^{-1}$  could have mechanical luminosities up to  $2 \times 10^{43}$  ergs s $^{-1}$  (Birzan et al. 2004). To produce the  $\sim 10^{59}$  ergs necessary to reheat the gas outside the core it is necessary that the AGN was active for the past  $\gtrsim 10^8$  yr (consistent with the radiative age determined by Giacintucci et al. 2007). Therefore, it is very likely that a central AGN outburst could be the main responsible for re-heating the gas between 8 and 30 kpc from the center, showing its signatures on the entropy profile (Fig. 10). Indeed, the lower entropy gas between 8 and 30 kpc may have been removed by the AGN outburst (e.g. Brüggen & Kaiser 2002).

## 8. CONCLUSIONS

In this paper we presented an analysis of a 40 ksec Chandra observation of the galaxy group AWM 5 (Albert et al. 1977). Although it does not meet the formal definition of a fossil group given in Jones et al. (2003), this group is a system with a dominant central galaxy, making it well suitable for a comparison with both “fossil” and normal groups. The main results from our analysis are:

- the abundance distribution shows a “hole” at the center, coincident with a CC. The maximum value of the abundance is at least a few times solar (at  $\sim 15 - 20$  kpc from the center). The presence of an abundance “hole” is not uncommon in groups and clusters of galaxies (e.g. Perseus cluster; Schmidt et al. 2002; Churazov et al. 2001; 2002) and can

be suggestive of metals being driven from the core;

- the derived deprojected electron density profile can be fit by two  $\beta$ -models. The inner one (at  $r < 13.4$  kpc) has  $\beta = 0.72^{+0.16}_{-0.11}$  and  $r_c = 5.7^{+1.8}_{-1.5}$  kpc). At  $r > 13.4$  kpc we derived  $\beta = 0.34 \pm 0.01$  and  $r_c = 31.3^{+5.8}_{-5.5}$  kpc. At  $r > 15$  kpc a power-law is also a good fit to the data with  $n_e \propto r^{-0.91 \pm 0.02}$  between 15 kpc and 300 kpc, a similar slope to that observed in cool groups (e.g. NGC1550, Sun et al. 2003) but much flatter than those measured in “fossil” groups (e.g. NGC6482, Khosroshahi et al. 2004; ESO3060170, Sun et al. 2004) and in clusters;
- we compared the X-ray and optical properties of the group members inside the Chandra field of view. Apart from NGC 6269 and NGC 6265 only three of the 12 group galaxies in the Chandra field of view were detected. Two other X-ray sources within  $1'$  ( $\sim 40$  kpc) of NGC 6269 have red, galaxy-like optical counterparts and are likely group members. We estimated  $M_{BH}$  for the group members from their  $K_s$  luminosity following the relation of Marconi & Hunt (2003). The ratio  $L_X/L_{Edd}$  is less than  $5 \times 10^{-6}$  showing that these black holes are accreting at highly sub-Eddington rates.
- we determined that the gas cooling time within the central 30 kpc of AWM 5 is smaller than the Hubble time, but only a small ( $r \sim 8$  kpc) CC is observed. This discrepancy suggests that the gas beyond  $\sim 8$  kpc has been re-heated;
- we find that heat conduction could be a significant source of re-heating in the AWM 5 core. Moreover, balance between heating expected from conduction and cooling due to X-ray emission requires large suppression (of a factor of at least  $\sim 100$ ) in the conductivity;
- we find evidence for past AGN activity (whose footprints are still observable as a radio source in the center of the cD galaxy NGC 6265). This is the most likely contributing source of re-heating for the central regions of AWM 5.
- we studied the properties of the ram pressure stripped tail in the group member NGC 6265. The galaxy is moving at  $M \approx 3.4^{+0.5}_{-0.6}$  in the group ICM. Moreover the physical length of the tail was measured to be  $\sim 42$  kpc.

We are grateful to M. Sun for providing us with the entropy profiles of the groups in his sample. We thank S. Giacintucci and M. Markevitch for useful discussions. We thank the anonymous referee for useful suggestions that helped to improve the presentation of the results in the paper.

## REFERENCES

- Albert, C., White, R., Morgan, W. 1977, ApJ, 211, 309
- Anders, E., Grevesse, N. 1989, in *Geochimica et Cosmochimica Acta*, vol. 53, p.197



- Arnaud, K. A. 1996, in “Astronomical Data Analysis Software and Systems V”, ASP Conference Series, Vol. 101, G. H. Jacoby and J. Barnes, eds., p. 17
- Ascasibar, Y. & Markevitch, M. 2006, *ApJ*, 650, 102
- Barnes, J. E. 1989, *Nature*, 338, 123
- Bettoni, D., Galletta, G., García-Burillo, S. 2003, *A&A*, 405, 5
- Birzan, L., Rafferty, D. A., McNamara, B. R., Wise, M. W., Nulsen, P. E. J. 2004, *ApJ*, 607, 800
- Böhringer, H., Fabian, A. C. 1989, *MNRAS*, 237, 1147
- Bondi, H. 1952, *MNRAS*, 112, 195
- Bregman, J. N., David, L. P. 1988, *ApJ*, 326, 639
- Brighenti, F., Mathews, W. G. 2002, *ApJ*, 573, 542
- Brüggen, M., Kaiser, C. R. 2002, *Nature*, 418, 301
- Burns, J. O., White, R. A., Hough, D. H. 1981, *AJ*, 86, 1
- Chandran, B. D. G., Cowley, S. C. 1998, *Phys. Rev. Lett.*, 80, 3077 (CC)
- Churazov, E., Brüggen, M., Kaiser, C. R., Böhringer, H., Forman, W. 2001, *ApJ*, 554, 261
- Churazov, E., Sunyaev, R., Forman, W., Böhringer, H. 2002, *MNRAS*, 332, 729
- Churazov, E., Forman, W., Jones, C., Böhringer, H. 2003, *ApJ*, 590, 225
- David, L. P., Jones, C., Forman, W. 1995, *ApJ*, 445, 578
- David, L. P., et al. 2001, *ApJ*, 557, 546
- Ellis, S. C., O’Sullivan, E. 2006, *MNRAS*, 367, 627
- Evrard, A. E., Metzler, C. A., Navarro, J. F. 1996, *ApJ*, 469, 494
- Fabian, A. C., Sanders, J. S., Allen, S. W., Crawford, C. S., Iwasawa, K., Johnstone, R. M., Schmidt, R. W., Taylor, G. B. 2003, *MNRAS*, 344, L43
- Finlator, K., et al. 2000, *AJ*, 120, 2615
- Forman, W., Nulsen, P., Heinz, S., Owen, F., Eilek, J., Vikhlinin, A., Markevitch, M., Kraft, R., Churazov, E., Jones, C. 2005, *ApJ*, 635, 894
- Forman, W., et al. 2007, *ApJ*, 665, 1057
- Gastaldello, F., Buote, D. A., Humphrey, P. J., Zappacosta, L., Bullock, J. S., Brighenti, F., Mathews, W. G. 2007, *ApJ*, 669, 158
- Giacintucci, S., Venturi, T., Murgia, M., Dallacasa, D., Athreya, R., Bardelli, S., Mazzotta, P., Sakira, D. J. 2007, *A&A*, 476, 99
- Hausman, M. A., Ostriker, J. P. 1978, *ApJ*, 224, 320
- Jones, C., Forman, W. 1999, *ApJ*, 511, 65
- Jones, L. R., Ponman, T. J., Forbes, D. A. 2000, *MNRAS*, 312, 139
- Jones, L. R., Ponman, T. J., Horton, A., Babul, A., Ebeling, H., Burke, D. J. 2003, *MNRAS*, 343, 627
- Kaastra, J. S. 1992, “An X-Ray Spectral Code for Optically Thin Plasmas” (Internal SRON-Leiden Report, updated version 2.0)
- Koranyi, D., Geller, M. 2002, *AJ*, 123, 100
- Khosroshahi, H. G., Jones, L. R., Ponman, T. J. 2004, *MNRAS*, 349, 1240
- Khosroshahi, H. G., Ponman, T. J., Jones, L. R. 2007, *MNRAS*, 377, 595
- Landau, L. D., Lifshitz, E. M., *Fluid Mechanics* (London: Pergamon), chapter 9
- Liedahl, D. A., Osterheld, A. L., Goldstein, W. H. 1995, *ApJ*, 438, 115
- Marconi, A., Hunt, L. K. 2003, *ApJ*, 589, L21
- Markevitch, M., et al., 2003a, *ApJ*, 583, 70
- Markevitch, M., Vikhlinin, A., Forman, W. R. 2003b, in ‘Matter and Energy in Clusters of Galaxies’, ASP Conference Proceedings, Vol. 301, held 23-27 April 2002, Chung-Li, Taiwan, S. Bowyer & C.-Y. Hwang eds.
- McNamara, B. R., Nulsen, P. E. J. 2007, *ARA&A*, 45, 117 *ApJ*, 583, 70
- Mulchaey, J. S., Zabludoff, A. I. 1999, *ApJ*, 514, 133
- Narayan, R., Medvedev, M. V. 2001, *ApJ*, 562, L129
- Navarro, J. F., Frenk, C. S., White, S. D. M. 1996, *ApJ*, 462, 563
- O’Sullivan, E., Vrtilek, J. M., Read, A. M., David, L. P., Ponman, T. J. 2003, *MNRAS*, 346, 525
- O’Sullivan, E., Vrtilek, J. M., Kempner, J. C., David, L. P., Houck, J. C. 2005, *MNRAS*, 357, 1134
- Ponman, T. J., Allan, D. J., Jones, L. R., Merrifield, M., McHardy, I. M., Lehto, H. J., Luppino, G. A. 1994, *Nature*, 369, 462
- Rasmussen, J., Ponman, T. J. 2007, *MNRAS*, 380, 1554
- Rechester, A. B., Rosenbluth, M. N. 1978, *Phys. Rev. Lett.*, 40, 38 (RR)
- Revnivtsev, M., Churazov, E., Sazonov, S., Forman, W., Jones, C. 2008, *A&A*, 490, 37
- Richards, G. T., et al. 2001, *AJ*, 121, 2308
- Sanderson, A. J. R., Ponman, T. J., Finoguenov, A., Lloyd-Davies, E. J., Markevitch, M. 2003, *MNRAS*, 340, 989
- Schmidt, R. W., Fabian, A. C., Sanders, J. S. 2002, *MNRAS*, 337, 71
- Simionescu, A., Werner, N., Finoguenov, A., Böhringer, H., Brüggen, M. 2008, *A&A*, in press, astro-ph 0709.4499
- Spitzer, L., Jr. 1962, *Physics of Fully Ionized Gases* (2nd ed.; New York: Interscience)
- Soria, R., Graham, A. W., Fabbiano, G., Baldi, A., Elvis, M., Jerjen, H., Pellegrini, S., Siemiginowska, A. 2006, *ApJ*, 640, 143
- Stark, A. A., Gammie, C. F., Wilson, R. W., Bally, J., Linke, R. A., Heiles, C., Hurwitz, M. 1992, *ApJS*, 79, 77
- Stewart, G. C., Fabian, A. C., Jones, C., Forman, W. 1984, *ApJ*, 285, 1
- Sun, M., Forman, W., Vikhlinin, A., Hornstrup, A., Jones, C., Murray, S. S. 2003, *ApJ*, 598, 250
- Sun, M., Forman, W., Vikhlinin, A., Hornstrup, A., Jones, C., Murray, S. S. 2004, *ApJ*, 612, 805
- Tozzi, P., Norman, C. 2001, *ApJ*, 546, 63
- Turatto, M., Cappellaro, E., Benetti, S. 1994, *AJ*, 108, 202
- Vikhlinin, A., McNamara, B. R., Hornstrup, A., Quintana, H., Forman, W., Jones, C., Way, M. 1999, *ApJ*, 520, L1
- Vikhlinin, A., Markevitch, M., Murray, S. S. 2001a, *ApJ*, 551, 160
- Vikhlinin, A., Markevitch, M., Forman, W., Jones, C. 2001b, *ApJ*, 555, L87
- Vikhlinin, A., Markevitch, M., Murray, S. S., Jones, C., Forman, W., Van Speybroeck, L. 2005, *ApJ*, 628, 655
- Zakamska, N. L., Narayan, R. 2003, *ApJ*, 582, 162

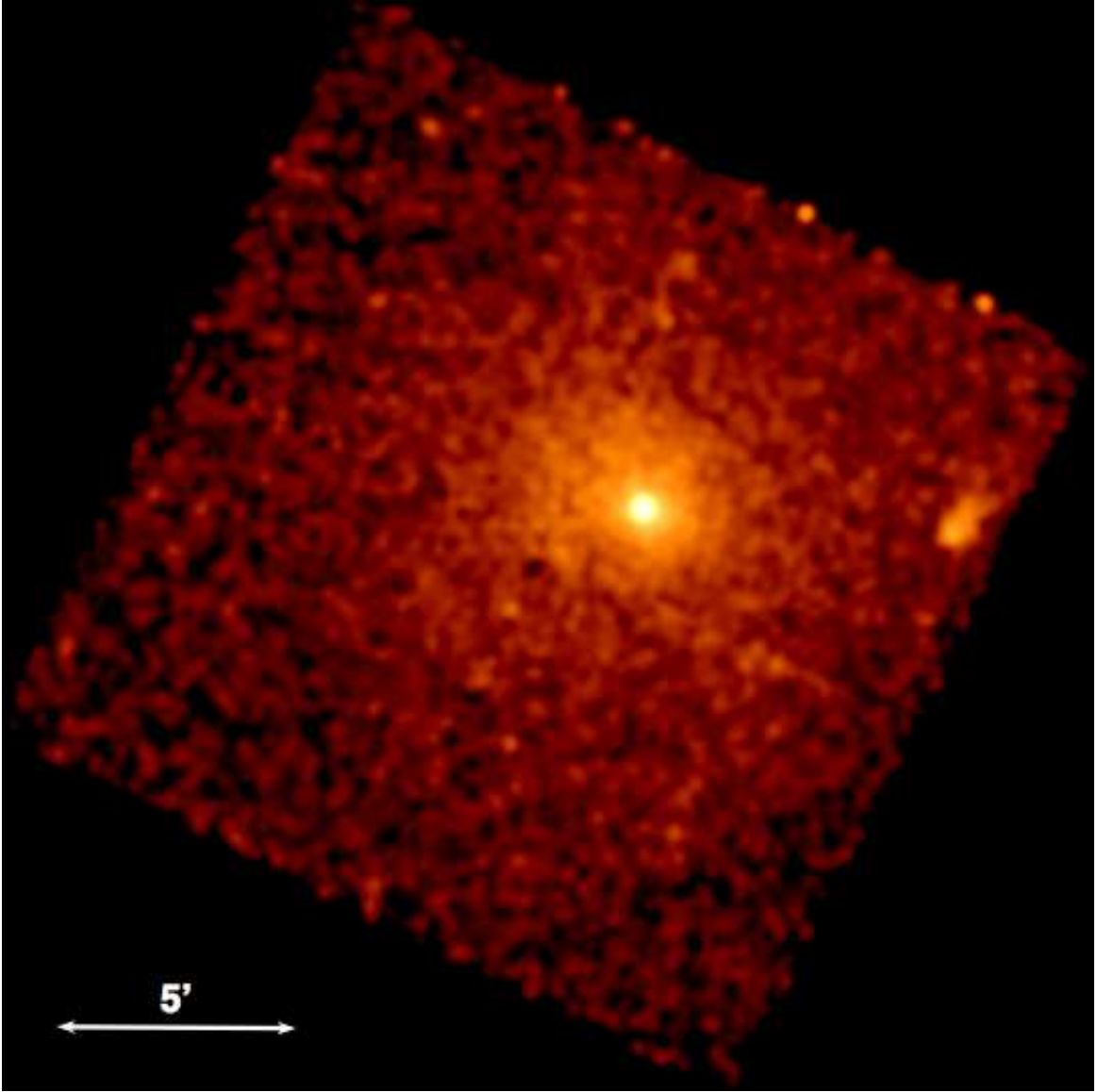


FIG. 1.— The 0.5–4 keV Chandra ACIS-I image of AWM 5, with the X-ray peak centered on the galaxy NGC 6269. The point sources were removed from the exposure corrected image and then smoothed with a 7 pixel ( $\sim 3.5''$ ) wide gaussian kernel. The group member NGC 6265 is visible  $\sim 6'$  to the west of NGC 6269, with a small ram-pressure stripped tail extending to the north-west.

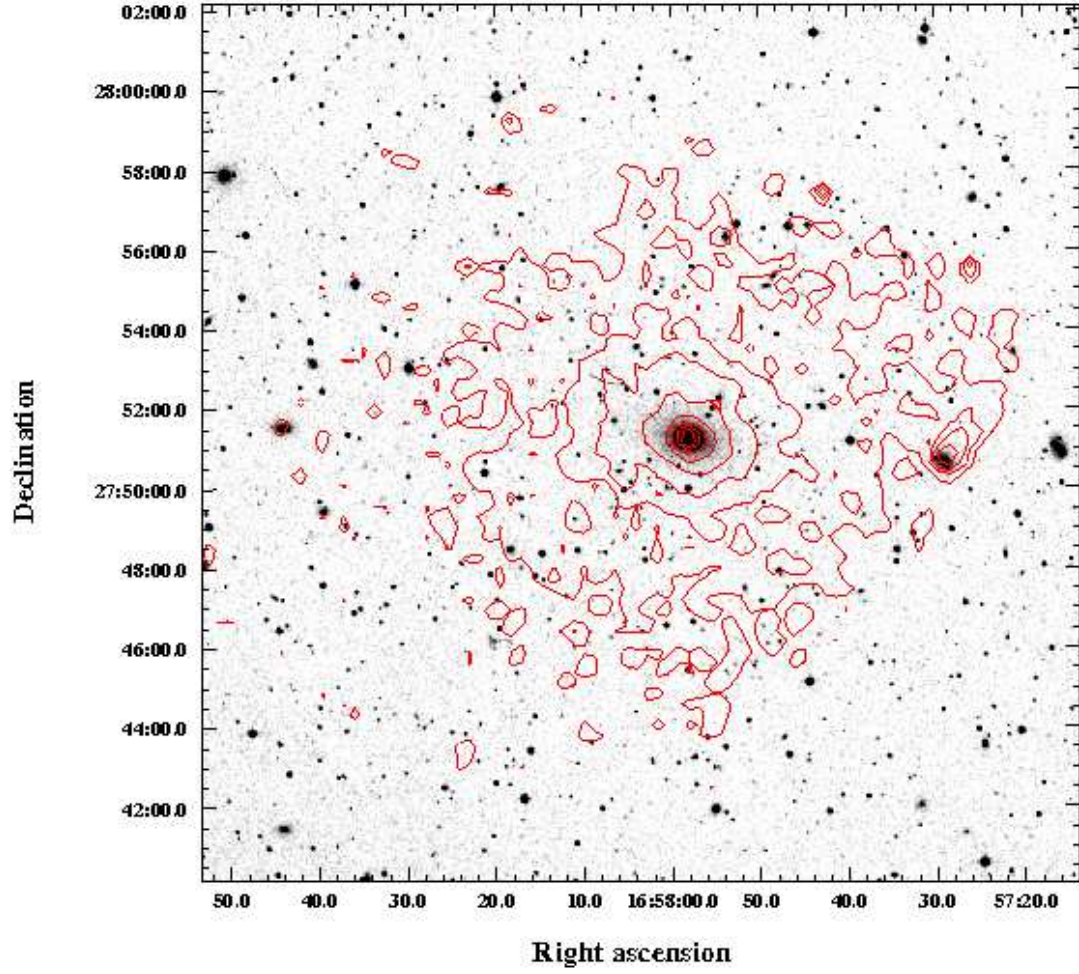


FIG. 2.— Optical DSS image of AWM5 with the 0.5–4 keV Chandra ACIS-I contours plotted in red. The central cD galaxy NGC 6269 is located in the peak of the X-ray emission. The group member NGC 6265 is the only other galaxy in the group associated with extended X-ray emission.

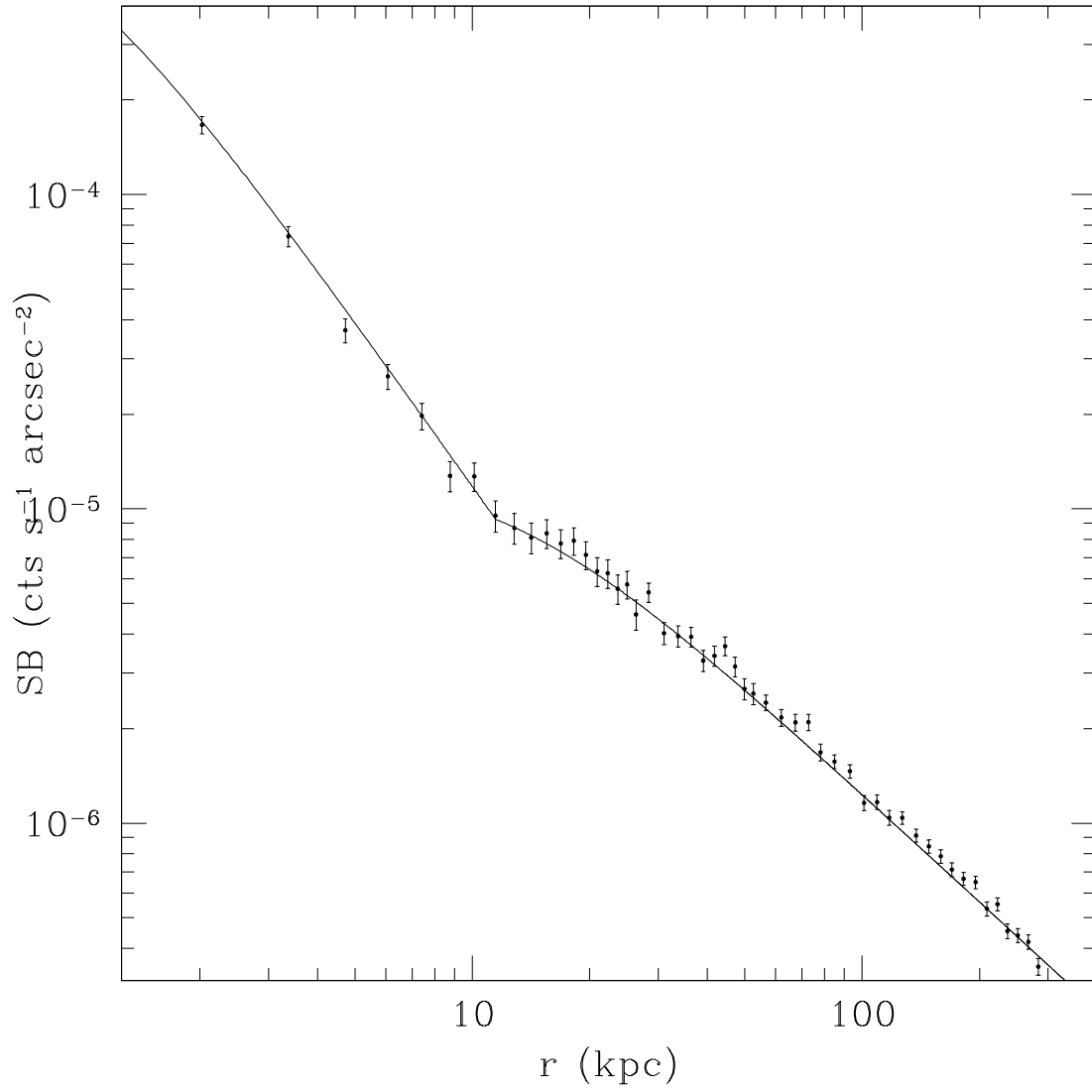


FIG. 3.— 0.5-4 keV Chandra ACIS-I surface brightness profile of the X-ray diffuse emission from AWM 5. The profile shows a break in the slope at  $\sim 10$  kpc from the center. The best fit double  $\beta$  model (plotted as a solid line) has  $r_c = 0.8 \pm 0.1$  kpc,  $\beta = 0.458^{+0.014}_{-0.013}$  at  $r < 11.4$  kpc, and  $r_c = 12.8^{+3.4}_{-0.9}$  kpc,  $\beta = 0.357 \pm 0.002$  at  $r > 11.4$  kpc.

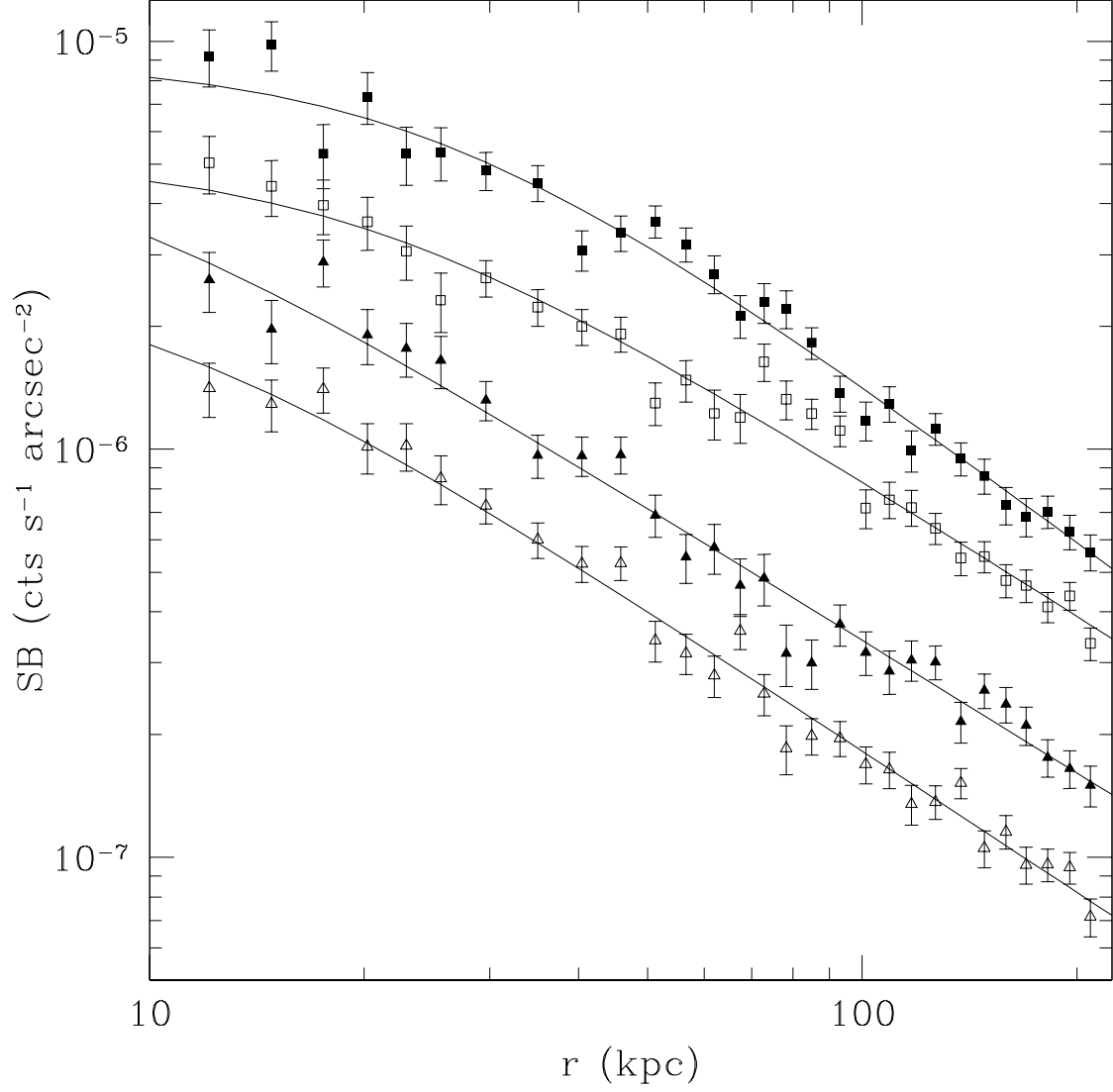


FIG. 4.— 0.5-4 keV Chandra ACIS-I surface brightness profile of the diffuse X-ray emission from AWM 5 in four azimuthal sectors: north=filled squares, east=open squares, south=filled triangles, west=open triangles. The eastern, southern and western profiles are offset from their original value for clarity. The corresponding best-fit  $\beta$  model is shown in the plot as well.

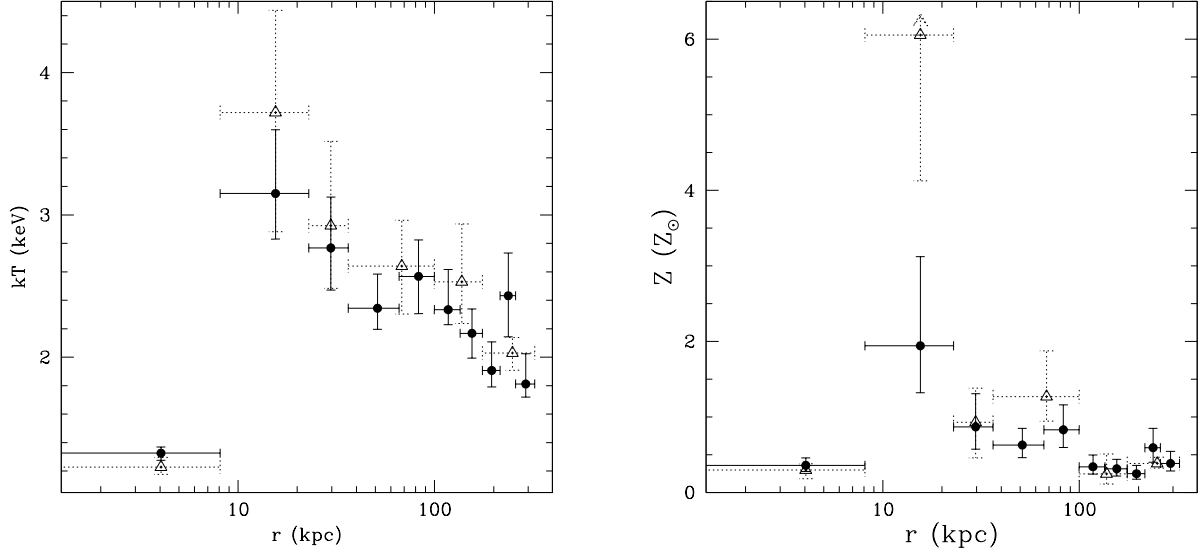


FIG. 5.— *Left:* Temperature profile for the X-ray gas observed in AWM 5. The projected temperature is plotted with filled circles and solid error bars, while the corresponding deprojected temperatures are plotted with open triangles and dotted error bars. A cooling core  $\sim 8$  kpc in size is visible in both the projected and deprojected profiles, with the latter showing a stronger temperature gradient toward the center. The two profiles are in general agreement at all radii and show a decline of the temperature from  $\sim 3.5$  keV, just outside the core, to  $\sim 2$  keV, at  $\sim 300$  kpc from the center. *Right:* Abundance profile for AWM 5. The symbols have the same meaning as in the left panel. Both the projected and deprojected profiles suggest an abundance “hole” interior to  $\sim 10$  kpc, where the temperature declines sharply.

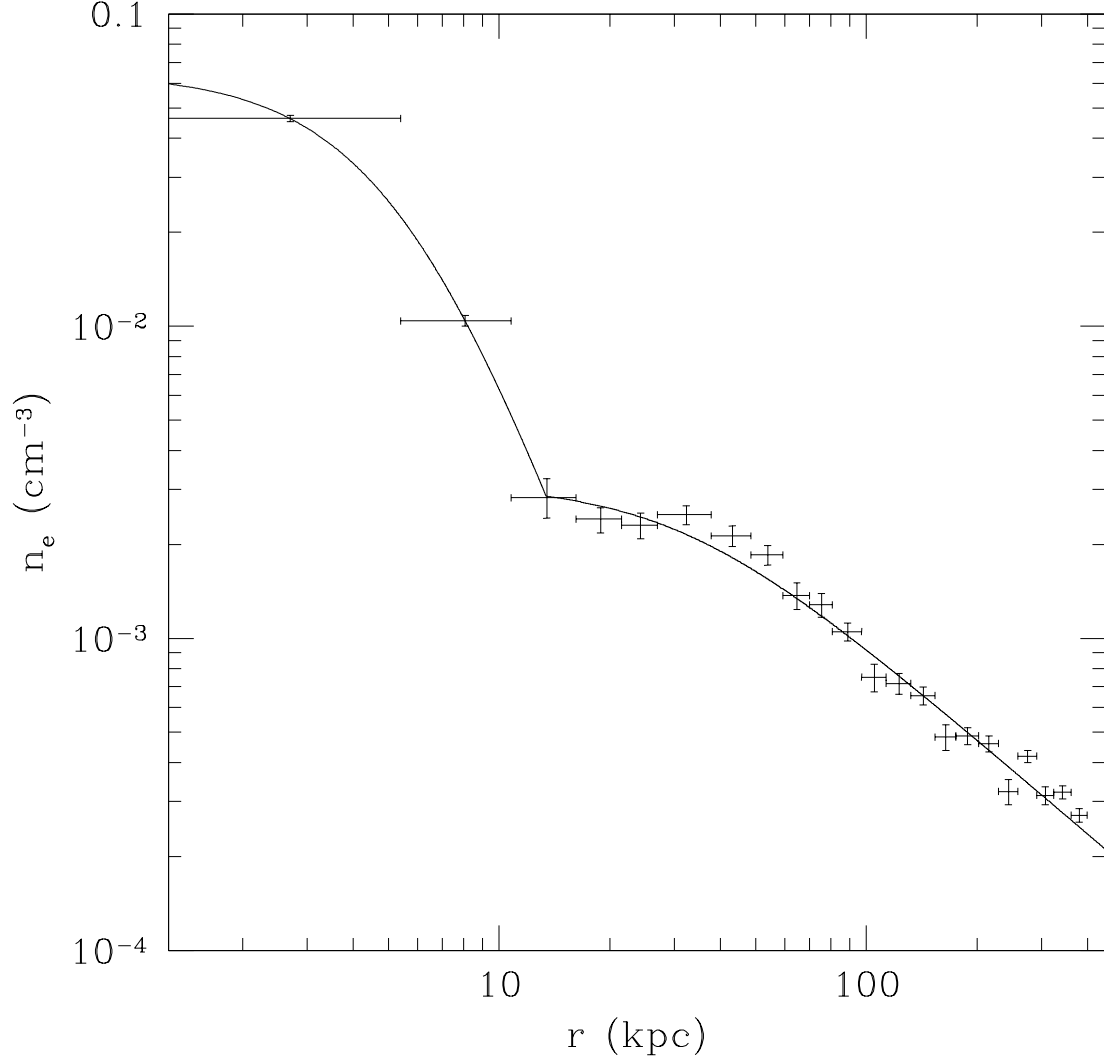


FIG. 6.— Electron density profile derived from a deprojection of the surface brightness. The density profile shows a clear break in the slope at  $r \sim 10$  kpc and can be fit by a double  $\beta$ -model. At  $r < 13.4$  kpc we obtain  $\beta = 0.72^{+0.16}_{-0.11}$  and  $r_c = 5.7^{+1.8}_{-1.5}$  kpc, while at  $r > 13.4$  kpc the best fit value of  $r_c$  is  $31.3^{+5.8}_{-5.5}$  kpc and  $\beta = 0.34 \pm 0.01$ . We found that  $n_e \propto r^{-0.91 \pm 0.02}$  between 30 kpc and 300 kpc.

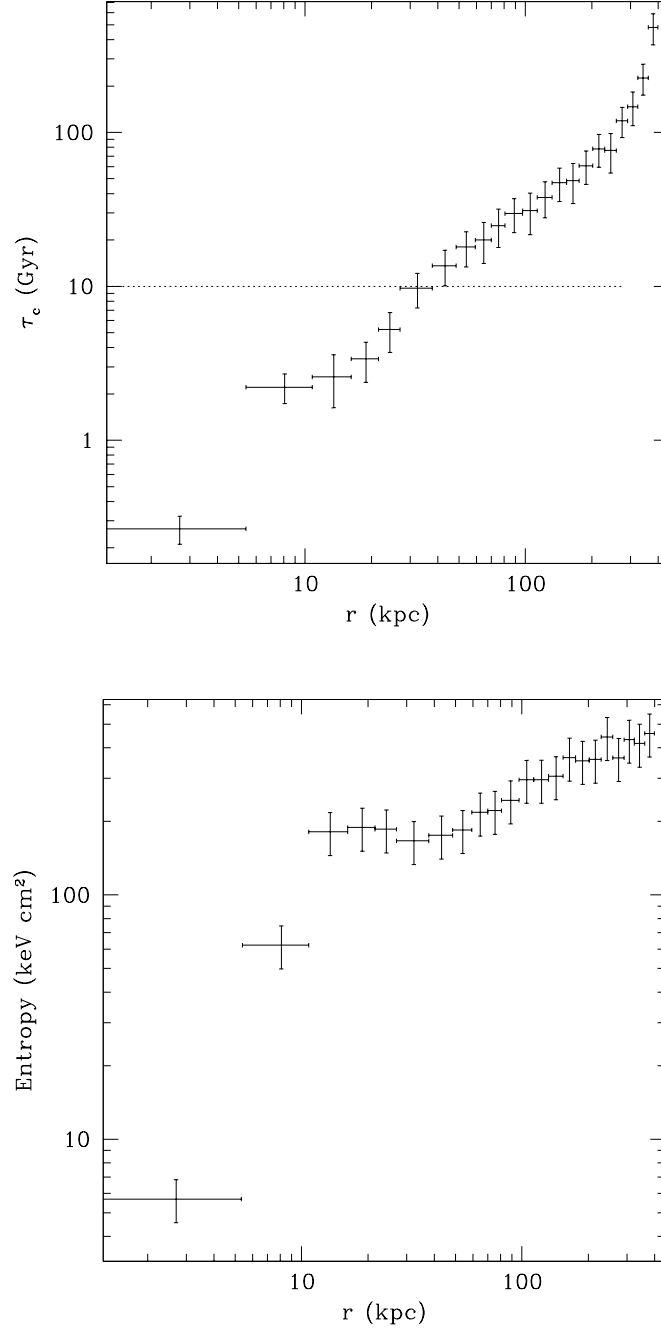


FIG. 7.— *Top:* Cooling time  $\tau_c$  of the gas as a function of the radial distance. The cooling time is less than a Hubble time inside the central  $\sim 30$  kpc. A comparison with the size of the cool core observed in the temperature profile ( $\sim 8$  kpc) may indicate that the central regions of AWM 5 were re-heated. *Bottom:* Entropy of the gas as a function of the distance from the center of the group. A flattening of the entropy profile is observed just outside the center and is just partly due to the cavities observed in correspondence with the radio lobes, and most likely related to the re-heating of the core.



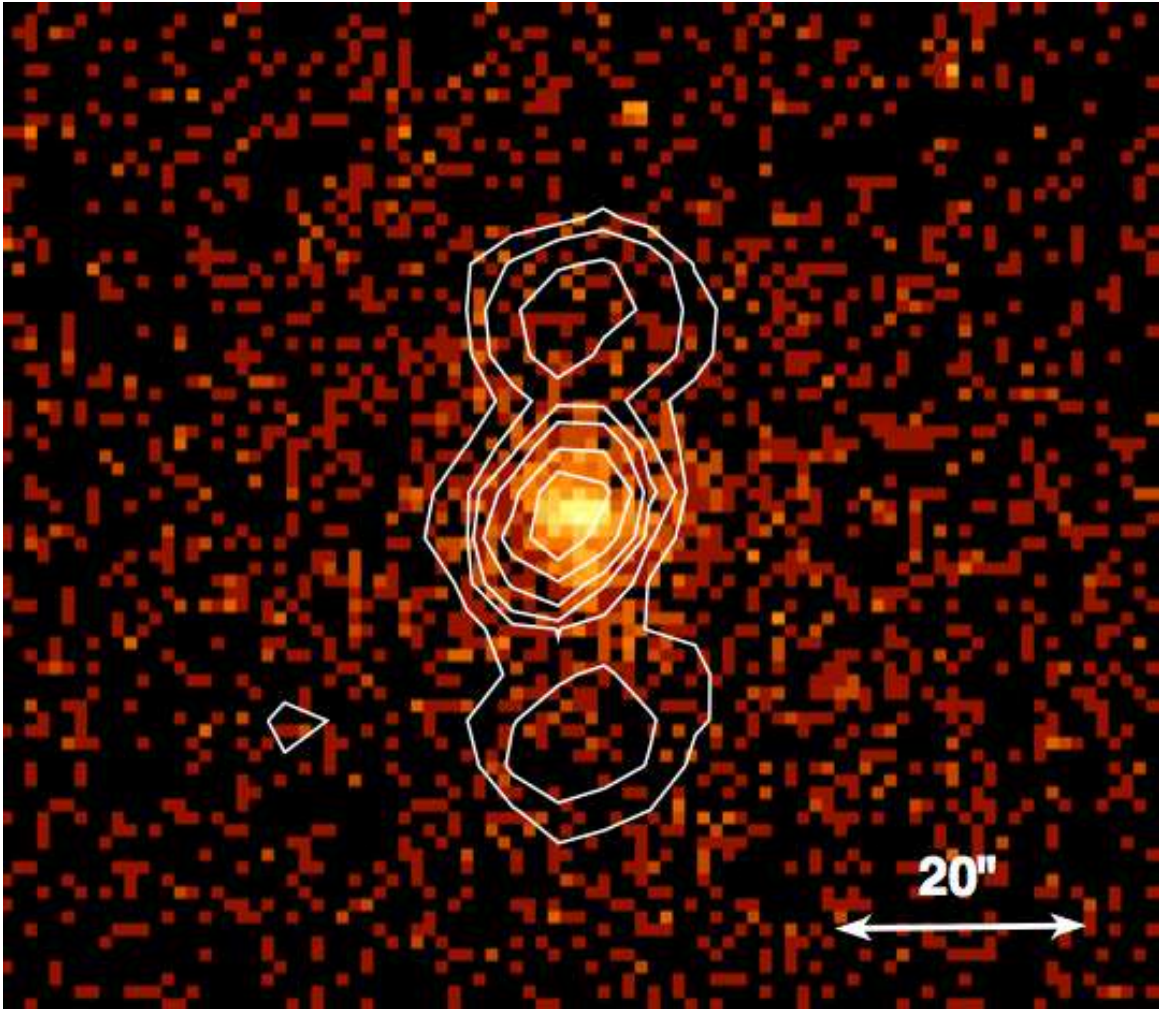


FIG. 8.— 1400 MHz radio contours from the FIRST superimposed on the ACIS-I 0.5-4 keV image. The radio source has a central nucleus ( $\sim 27$  mJy) coincident with the group core, with north-south radio lobes ( $\sim 8$  and  $\sim 10$  mJy) extending  $25''$  ( $\sim 17$  kpc) from the center.

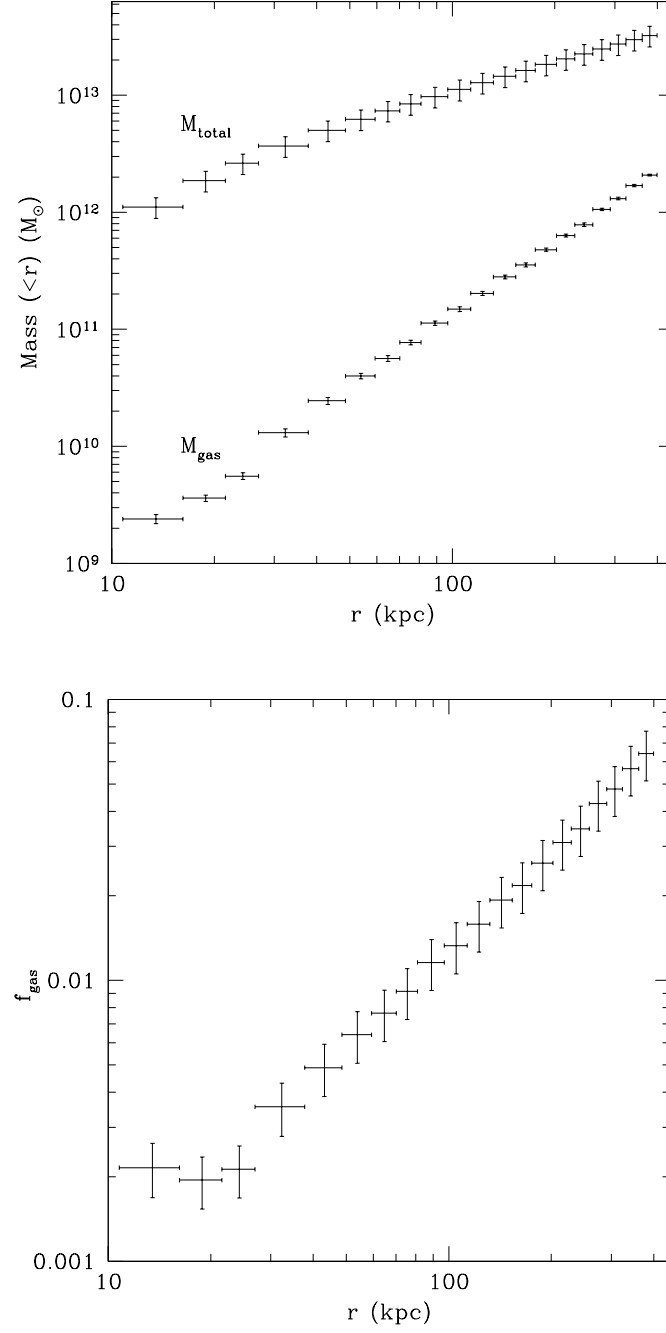


FIG. 9.— *Top*: Total gravitating mass and X-ray gas mass enclosed within a radius  $r$  in the AWM 5 group. *Bottom*: Fraction of the gas mass over the total gravitating mass as a function of the distance from the center. The gas fraction is flat within the central 30 kpc and increases afterwards reaching a maximum value of 6.5% at  $\sim 380$  kpc.

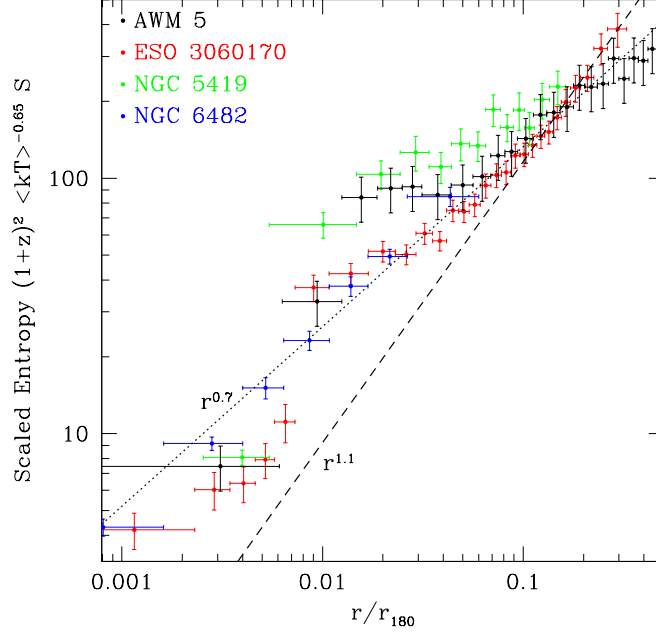


FIG. 10.— Scaled entropy profiles for AWM 5 compared with other groups (ESO3060170, NGC 5419, NGC 6482). The entropy profile of AWM 5 is generally flatter than the other groups ( $\propto r^{0.7}$ , dotted line) and also from the slope ( $\propto r^{1.1}$ , plotted as a dashed line) predicted by cluster simulations (Tozzi & Norman 2001). The flattening of the entropy profile just outside the core of AWM 5 ( $0.01r_{180} \leq r \leq 0.05r_{180}$ ) has been observed also in other fossil groups lacking a cool core (e.g. NGC 5419, ESO3060170) and is most likely related to the re-heating of the cores.

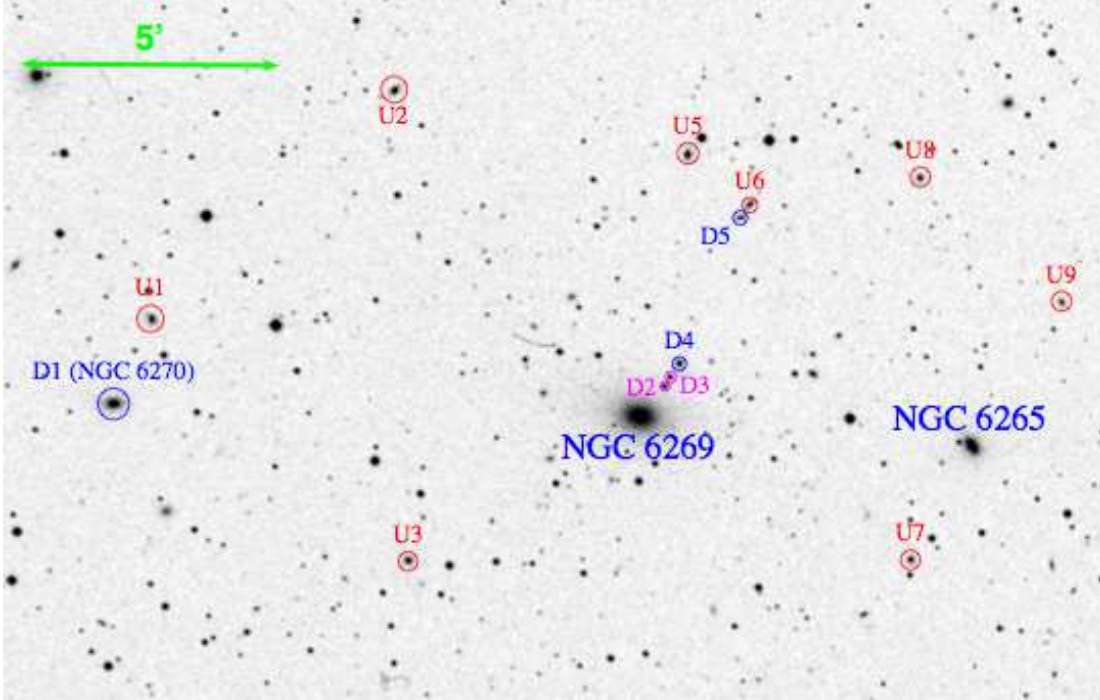


FIG. 11.— ESO Digitized Sky Survey R-band image of the group AWM 5. The blue circles refer to the group members (with a confirmed radial velocity from Koranyi & Geller 2002) with a detected X-ray counterpart from Chandra ACIS-I, while the group members without a Chandra counterpart are shown with red circles. The two galaxies indicated with a magenta circle do not have a determination of the radial velocity, however they are detected in the Chandra image and look to be part of an alignment together with the source D4, pointing toward NGC 6269.

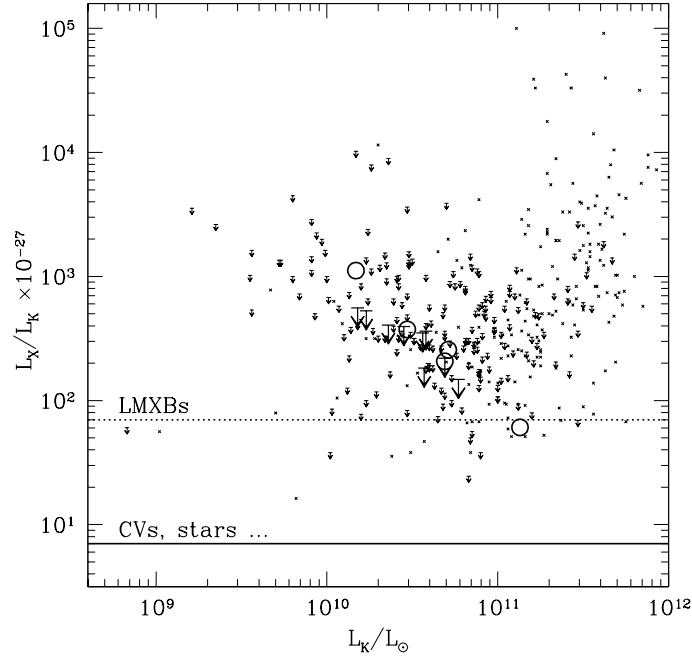


FIG. 12.— Infrared luminosity ( $L_{K_s}$ , expressed in solar units) vs. the ratio of the X-ray luminosity over  $L_{K_s}$  in the AWM 5 members (big circles and big bold upper limits) and in a sample of early-type galaxies from Ellis & O’Sullivan (small crosses and small upper limits). The maximum contribution to the X-ray emission expected from CVs and normal stars (solid line) and from LMXBs (dotted line) is plotted as well. The AWM 5 group members follow the distribution of early-type galaxies and are well above the contribution expected from CVs and stars. All the group members with detected X-ray emission, except D1, are also not consistent with emission coming exclusively from LMXBs.

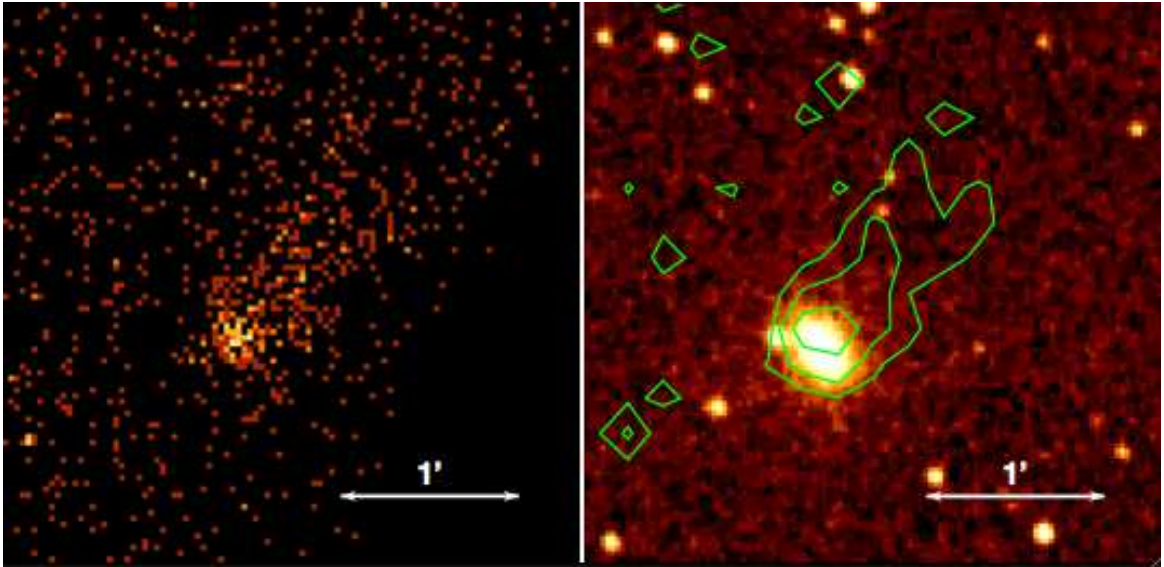


FIG. 13.— *Left*: X-ray emission (0.5-2 keV;  $4''$  bins) of ram pressure stripped gas from NGC 6265. *Right*: X-ray contours superimposed on the optical DSS image. The X-ray tail is 40 kpc long (projected on the sky).

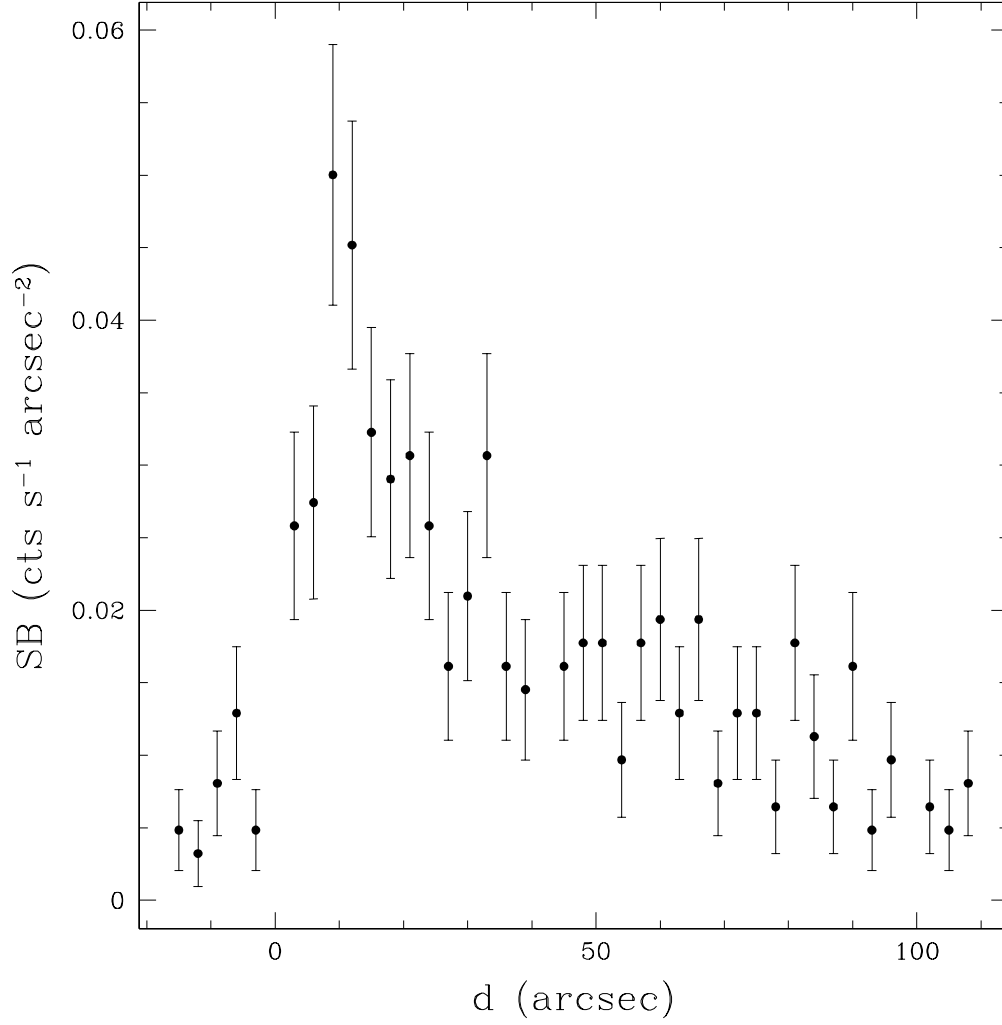


FIG. 14.— Surface brightness profile along the X-ray gas stream around NGC 6265. The zero on the X-axis corresponds to the leading edge of the X-ray emission, where a sudden drop in surface brightness of a factor of 3-4 is observed.

TABLE 1  
BEST FIT  $\beta$  MODELS FOR THE SURFACE BRIGHTNESS  
PROFILE WEDGES OF AWM 5

Wedge Orientation	$\chi^2/dof$	$\beta$	$r_c$ (kpc)
East	37.7/26	$0.352 \pm 0.005$	$19.7^{+5.9}_{-5.3}$
North	30.8/26	$0.383 \pm 0.006$	$24.7^{+5.1}_{-4.6}$
South	34.2/26	$0.347 \pm 0.005$	$7.0^{+3.8}_{-3.1}$
West	29.9/26	$0.359 \pm 0.005$	$9.4^{+3.2}_{-3.6}$

TABLE 2  
 GALAXIES WITH VELOCITIES CONSISTENT WITH THE AWM 5 GROUP WITHIN THE CHANDRA ACIS-I FIELD OF VIEW AND  
 RELATIVE OPTICAL-INFRARED PROPERTIES. THE OPTICAL COLORS ARE TAKEN FROM THE THIRD DATA RELEASE OF SDSS  
 (ABAZAJIAN ET AL. 2005), WHILE THE INFRARED ARE FROM 2MASS. THE RADIAL VELOCITIES ARE FROM KORANYI &  
 GELLER (2002).

#	RA (J2000)	Dec (J2000)	$u$	$g$	$r$	$i$	$z$	B	$\log L_B$ ( $L_\odot$ )	$K_s$	$\log L_{K_s}$ ( $L_\odot$ )	$v_r$ (km s $^{-1}$ )
N6269	16:57:58.1	+27:51:16	15.5	13.5	12.6	12.1	11.7	14.1	10.87	9.40	11.91	10460
N6265	16:57:29.1	+27:50:39	16.7	14.7	13.8	13.4	13.0	15.3	10.39	10.75	11.37	9725
D1	16:58:44.1	+27:51:32	17.2	15.2	14.3	13.9	13.6	15.8	10.19	11.35	11.13	9720
D2	16:57:55.9	+27:51:52	20.0	17.5	16.1	15.0	14.5	18.3	9.19	12.40	10.71	(10670)
D3	16:57:55.4	+27:52:01	20.1	17.6	16.2	15.1	14.5	18.4	9.15	12.45	10.69	(10670)
D4	16:57:54.6	+27:52:17	18.8	16.8	16.0	15.5	15.2	17.3	9.59	13.00	10.47	10670
D5	16:57:49.2	+27:55:06	18.6	16.9	16.1	15.7	15.4	17.4	9.55	13.75	10.17	10371
U1	16:58:40.8	+27:53:10	18.3	16.5	15.6	15.1	14.8	17.0	9.71	12.76	10.56	10722
U2	16:58:19.4	+27:57:35	18.3	16.3	15.4	14.9	14.6	16.9	9.75	12.24	10.77	9976
U3	16:58:18.3	+27:48:30	18.5	16.7	15.8	15.4	15.0	17.3	9.59	13.05	10.45	10194
U4	16:57:55.1	+27:41:58	18.0	16.1	15.2	14.7	14.4	16.7	9.83	12.44	10.69	10977
U5	16:57:53.8	+27:56:18	18.2	16.4	15.5	15.1	14.8	16.9	9.75	12.73	10.58	11510
U6	16:57:48.4	+27:55:20	19.0	17.3	16.4	16.0	15.7	17.9	9.35	13.59	10.23	11159
U7	16:57:34.7	+27:48:28	18.6	16.8	15.9	15.5	15.2	17.4	9.55	12.74	10.57	11088
U8	16:57:33.5	+27:55:50	18.9	16.9	16.0	15.5	15.2	17.5	9.51	13.26	10.36	11237
U9	16:57:21.3	+27:53:26	19.1	17.3	16.4	16.0	15.7	17.9	9.35	13.71	10.18	10822

TABLE 3

BLACK HOLE MASSES, X-RAY LUMINOSITIES AND BONDI ACCRETION RATES FOR THE AWM 5 GROUP MEMBERS IN THE ACIS-I FIELD OF VIEW. THE BLACK HOLE MASSES WERE DERIVED FROM  $L_{K_s}$  FOLLOWING MARCONI & HUNT (2003). THE BONDI ACCRETION RATE (BONDI 1952) WAS DETERMINED ASSUMING THE TEMPERATURE AND DENSITY OF THE GAS AT THE POSITION OF EACH GALAXY AS DERIVED IN § 3.4 AND THEREFORE CAN BE CONSIDERED UPPER LIMITS APART FROM THE CASE OF THE CENTRAL GALAXY NGC 6269. THE BONDI LUMINOSITIES WERE COMPUTED ASSUMING AN ACCRETION EFFICIENCY  $\eta = 0.1$ .

#	$M_{BH}$ ( $M_{\odot}$ )	$\log L_{0.3-10\ keV}$ ( $\text{erg s}^{-1}$ )	$L_{0.3-10\ keV}/L_{Edd}$	$\dot{M}_{Bondi}$ ( $M_{\odot}\ \text{yr}^{-1}$ )	$\log L_{Bondi}$ ( $\text{erg s}^{-1}$ )
N6269	$1.6 \times 10^9$	< 40.73	$2.6 \times 10^{-7}$	$6.0 \times 10^{-3}$	43.53
N6265	$6.0 \times 10^8$	< 40.35	$2.9 \times 10^{-7}$	< $5.7 \times 10^{-7}$	< 39.51
D1	$2.8 \times 10^8$	39.91	$2.3 \times 10^{-7}$	< $1.3 \times 10^{-4}$	< 41.87
D2	$10^8$	40.12	$10^{-6}$	< $1.7 \times 10^{-5}$	< 40.97
D3	$10^8$	40.01	$10^{-6}$	< $1.7 \times 10^{-5}$	< 40.97
D4	$6 \times 10^7$	40.04	$1.4 \times 10^{-6}$	< $5.9 \times 10^{-6}$	< 40.53
D5	$2.5 \times 10^7$	40.22	$5 \times 10^{-6}$	< $1.0 \times 10^{-6}$	< 39.77
U1	$6.3 \times 10^7$	< 40.11	< $1.6 \times 10^{-6}$	< $6.6 \times 10^{-6}$	< 40.57
U2	$1.1 \times 10^8$	< 39.94	< $6.2 \times 10^{-7}$	< $2.0 \times 10^{-5}$	< 41.06
U3	$6 \times 10^7$	< 40.05	< $1.4 \times 10^{-6}$	< $6.0 \times 10^{-6}$	< 40.53
U4	$10^8$	< 40.03	< $8.2 \times 10^{-7}$	< $1.7 \times 10^{-5}$	< 40.97
U5	$6.3 \times 10^7$	< 40.14	< $1.7 \times 10^{-6}$	< $6.6 \times 10^{-6}$	< 40.57
U6	$3.2 \times 10^7$	< 39.95	< $2.1 \times 10^{-6}$	< $1.7 \times 10^{-6}$	< 39.98
U7	$6.3 \times 10^7$	< 39.83	< $8.2 \times 10^{-7}$	< $6.6 \times 10^{-6}$	< 40.57
U8	$4 \times 10^7$	< 39.97	< $1.8 \times 10^{-6}$	< $2.7 \times 10^{-6}$	< 40.18
U9	$2.5 \times 10^7$	< 39.93	< $2.6 \times 10^{-6}$	< $1.0 \times 10^{-6}$	< 39.77